AD-A108 691 SOUTHWEST RESEARCH INST SAN ANTONIO TX F/G 20/11
FATIGUE MICROCRACK BEHAVIOR UNDER THE INFLUENCE OF SURFACE RESI--ETC(U)
OCT 81 J E HACK, G R LEVERANT N00014-78-C-0674
UNCLASSIFIED NL

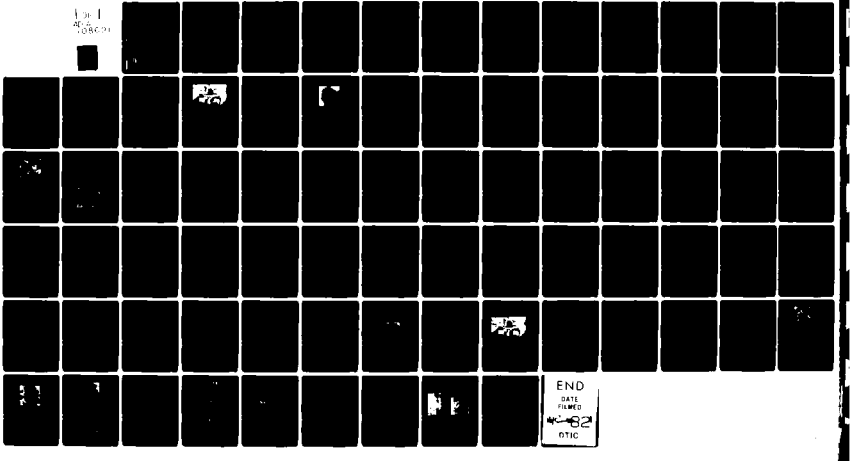

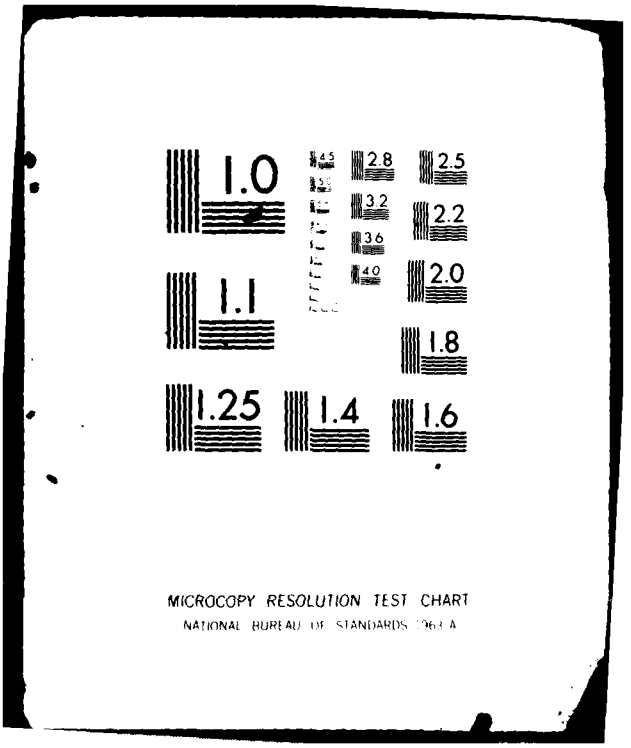
1.0
1.1
1.25
1.4
1.6
1.8
2.0
2.2
2.5
2.8
3.2
3.6
4.0
4.5
MICROCOPY RESOLUTION TEST CHART
NATIONAL BUREAU OF STANDARDS 1963 A

AD A108691

FATIGUE MICROCRACK BEHAVIOR UNDER THE INFLUENCE OF SURFACE RESIDUAL STRESSES

J. E. Hack and G. R. Leverant
Southwest Research Institute
P. O. Drawer 28510
San Antonio, Texas 78284

INTERIM REPORT for Period August 1, 1980 - August 31, 1981
Contract N00014-78-C-0674

Reproduction in whole or in part is permitted
for any purpose of the United State Government. Distribution is unlimited.

Prepared for
OFFICE OF NAVAL RESEARCH
800 North Quincy Street
Arlington, Virginia 22217

October 30, 1981

DTIC
DEC 18 1981
A

DTIC FILE COPY

SOUTHWEST RESEARCH INSTITUTE
SAN ANTONIO HOUSTON

FATIGUE MICROCRACK BEHAVIOR UNDER THE INFLUENCE OF SURFACE RESIDUAL STRESSES

J. E. Hack and G. R. Leverant
Southwest Research Institute
P. O. Drawer 28510
San Antonio, Texas 78284

INTERIM REPORT for Period August 1, 1980 - August 31, 1981
Contract N00014-78-C-0674

Prepared for
OFFICE OF NAVAL RESEARCH
800 North Quincy Street
Arlington, Virginia 22217

October 30, 1981

ELECTE
DEC 18 1981
A

Approved:

U. S. Lindholm, Director
Department of Materials Sciences

81 12 17060

Unclassified

SECURITY CLASSIFICATION OF THIS PAGE (When Data Entered)

REPORT DOCUMENTATION PAGE		READ INSTRUCTIONS BEFORE COMPLETING FORM
1. REPORT NUMBER	2. GOVT ACCESSION NO. AD-A108 654	3. RECIPIENT'S CATALOG NUMBER
4. TITLE (and Subtitle) FATIGUE MICROCRACK BEHAVIOR UNDER THE INFLUENCE OF SURFACE RESIDUAL STRESSES		5. TYPE OF REPORT & PERIOD COVERED Interim Report 8/1/80 - 8/31/81
		6. PERFORMING ORG. REPORT NUMBER 02-5382
7. AUTHOR(s) J. E. Hack G. R. Leverant		8. CONTRACT OR GRANT NUMBER(s) N00014-78-C-0674
9. PERFORMING ORGANIZATION NAME AND ADDRESS Southwest Research Institute P. O. Drawer 28510 San Antonio, TX 78284		10. PROGRAM ELEMENT, PROJECT, TASK AREA & WORK UNIT NUMBERS Project Element 122201 NR031-812/6-23-78(471)
11. CONTROLLING OFFICE NAME AND ADDRESS Office of Naval Research 800 North Quincy Street Arlington, VA 22217		12. REPORT DATE October 30 1981
		13. NUMBER OF PAGES 32 + prelims and appendix
14. MONITORING AGENCY NAME & ADDRESS(if different from Controlling Office)		15. SECURITY CLASS. (of this report) Unclassified
		15a. DECLASSIFICATION DOWNGRADING SCHEDULE

16. DISTRIBUTION STATEMENT (of this Report)

Reproduction in whole or in part is permitted for any purpose of the United States Government. Distribution is unlimited.

17. DISTRIBUTION STATEMENT (of the abstract entered in Block 20, if different from Report)

18. SUPPLEMENTARY NOTES

19. KEY WORDS (Continue on reverse side if necessary and identify by block number)

Fatigue	Titanium
Microcrack	Steel
Residual Stress	Surface Crack Opening Displacement
Environmental Effects	Stress Intensity

20. ABSTRACT (Continue on reverse side if necessary and identify by block number)

Direct observations of the surface crack opening displacement (SCOD) of surface microcracks (2c ≈ 400 μ) have been made on samples of 4140 and HY-130 steels under both cyclic and static loading conditions. Preliminary observations indicate that small cracks which reside entirely within the zone of shot-peen-induced compressive residual stress remain completely closed, even at applied loads approaching the bulk yield stress in HY-130. Results of SCOD measurements on HY-130 specimens which were cycled in an aqueous 3.5%

DD FORM 1 JAN 73 1473 EDITION OF 1 NOV 65 IS OBSOLETE

Unclassified

SECURITY CLASSIFICATION OF THIS PAGE (When Data Entered)

NaCl solution show a large reduction in SCOD (effective ΔK) due to a wedging open of the crack by oxides on the crack faces. As far as we know, the results of these near-threshold, low R-ratio tests represent the first direct observations of oxide wedging effects in microcracks and are consistent with independent data for large crack behavior.

Predictions using the analytical approach developed earlier in this program give excellent correlation with experimental observations in 4140 steel in the absence of surface residual stresses. Similar analyses are currently being conducted for HY-130. In addition, a boundary-integral program for the direct calculation of crack face displacements is being used to determine complete crack opening profiles in the presence of a surface residual stress gradient.

FOREWORD

The research reported herein was conducted by Southwest Research Institute of San Antonio, Texas, under Contract N00014-78-C-0674. The report summarizes work accomplished during the period of August 1980 through August 1981. Dr. Bruce MacDonald was the ONR Program Manager. The work was conducted under the general supervision of Dr. Gerald R. Leverant, SwRI Project Manager, with assistance from Mr. John E. Hack, who acted as Principal Engineer. Special acknowledgement is due to Dr. David L. Davidson, who conducted the in-situ SEM loading experiments and, along with Dr. Richard A. Page and Mr. Stephen J. Hudak, Jr., offered many pertinent suggestions. The assistance of Messrs. Harold Saldana and Victor Aaron in sample preparation and testing is greatly appreciated.

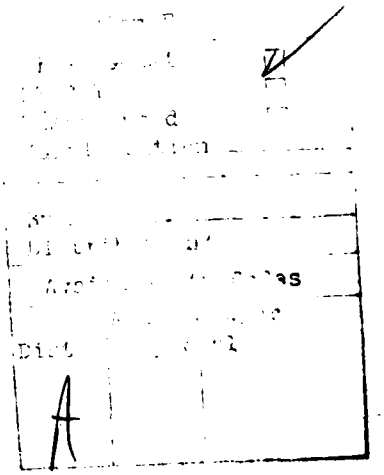

TABLE OF CONTENTS

LIST OF TABLES

LIST OF FIGURES

LIST OF FIGURES (CONT.)

I. INTRODUCTION

Fatigue cracks in metals generally nucleate at or near a free surface. Since the initial growth rates of microcracks are in the near-threshold region ($\sim 10^{-6}$ mm/cycle), fatigue cracks spend a significant portion of their lifetimes in the near-surface region. Thus, the residual stress state at the surface produced by common mechanical and thermal processing can have a marked effect on the fatigue behavior of a material. In addition, aggressive environments can dramatically change crack growth behavior in the near-threshold region, either acting alone or in conjunction with an imposed surface residual stress state. This report details current results of an ongoing program to quantify the relationship between surface condition, environment, and fatigue microcrack growth.

The approach utilized in this program is to quantify the effects of surface residual stresses and environment on surface crack opening displacement (SCOD) behavior. Since COD can be directly related to crack growth rate [1,2], these data can be used to correlate these parameters with fatigue behavior. A loading stage which operates in-situ in an SEM is being used to generate SCOD vs. load data for microcracks in Ti-6Al-4V and 4140 and HY-130 steels.

Current results of experimental observations are presented herein that compare SCOD behavior in the presence of various levels of compressive stress. In addition, SCOD behavior is compared for air and salt-water environments. A previously-developed analytical approach for the prediction of SCOD behavior has been applied to cracked steel specimens. The results are compared to those generated previously in a titanium alloy.

Furthermore, the preliminary application of a boundary integral program for the calculation of crack profiles under the influence of surface residual stresses is also discussed. A detailed description of the analytical approach is presented in a paper which has been accepted for an ASTM Special Technical Publication on Residual Stress Effects in Fatigue. A copy of the paper is attached as an appendix.

II. DIRECT OBSERVATION OF SCOD VS. LOAD BEHAVIOR

A. Experimental Procedure

Experiments were performed on 4140 and HY-130 steels. The 4140 specimens were machined from a 6.25 mm rolled plate, while the HY-130 specimens were machined from a 50.8 mm rolled plate in the quenched-and-tempered condition. The microstructures of the two steels are shown in Figure 1, while the alloy compositions are summarized in Table I.

A cantilever beam fatigue specimen was used to promote surface crack initiation. Figure 2 shows the straight-sided specimen. A small, roughly semicircular starter notch (≈ 125 μ long and 60 μ deep) was placed in the center of the gage by electrical discharge machining (EDM). It can be seen from the figure that slots are incorporated in the grip sections to allow for fixturing into the SEM tensile loading stage after the initiation of cracks in the bending rig.

The SEM loading stage, developed at SwRI [3], is shown in Figure 3. The stage is capable of cyclically loading a specimen in tension-tension at loads up to 3800 N, at frequencies ranging from 0-5 Hz, while maintaining the area of interest within the viewing screen of the SEM and in focus. Crack behavior can be videotaped and replayed for analysis of crack opening displacement response. In addition, samples can be statically loaded in tension at loads up to 4900 N.

A sample of 4140 and several HY-130 samples were notched by EDM and precracked in bending between the strain limits of 0.15 ± 0.25% (0.10 ± 0.18% for the 4140). The HY-130 specimens were then shot-peened at an intensity of 0.011 A. All of the specimens were then metallographically

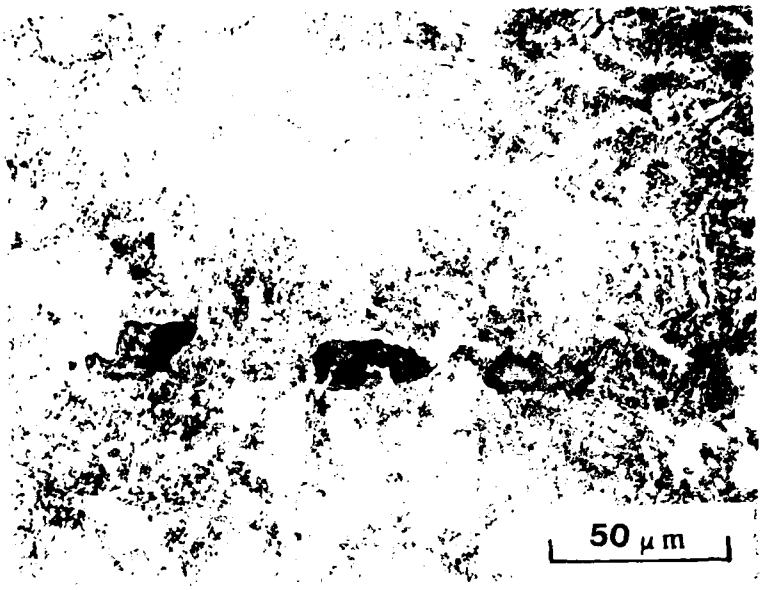

(a) 4140

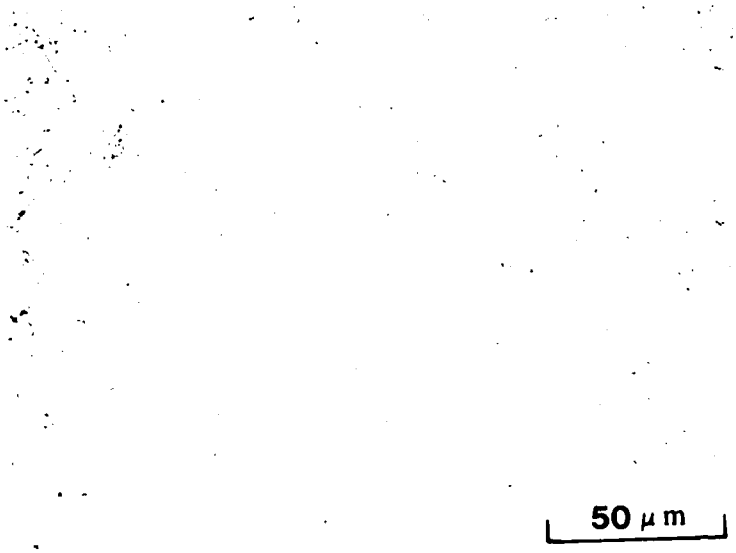

(b) HY-130

FIGURE 1. MICROSTRUCTURES OF ALLOYS STUDIED

TABLE I

NOMINAL ALLOY COMPOSITIONS

Material	Element	Wt-Pct
4140	C	0.38 - 0.43
	Mn	0.75 - 1.00
	P (max)	0.035
	S (max)	0.04
	Si	0.15 - 0.30
	Cr	0.80 - 1.10
	Mo	0.15 - 0.25
HY-130	C	0.12
	Mn	0.60 - 0.90
	P (max)	0.01
	S (max)	0.015
	Si	0.20 - 0.35
	Ni	4.75 - 5.25
	Cr	0.40 - 0.70
	Mo	0.30 - 0.65
	V	0.05 - 0.10

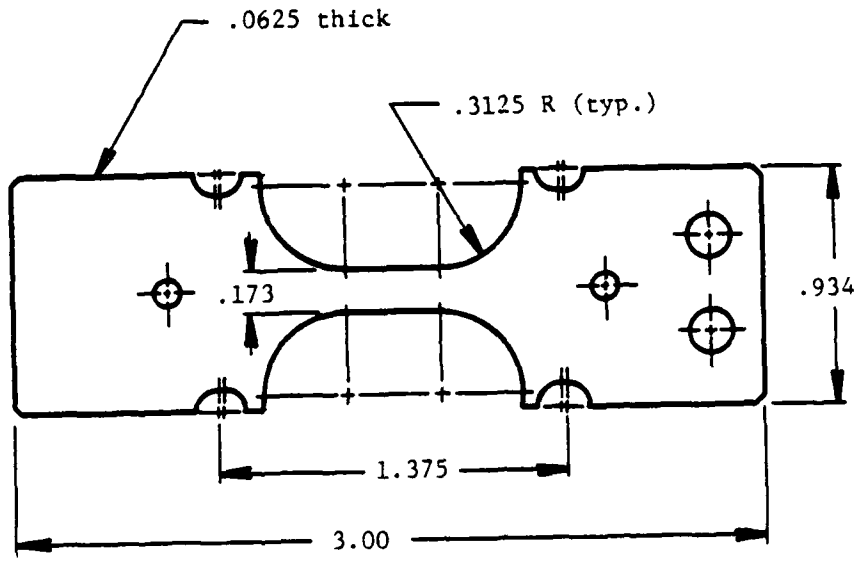

FIGURE 2. SPECIMEN DESIGN

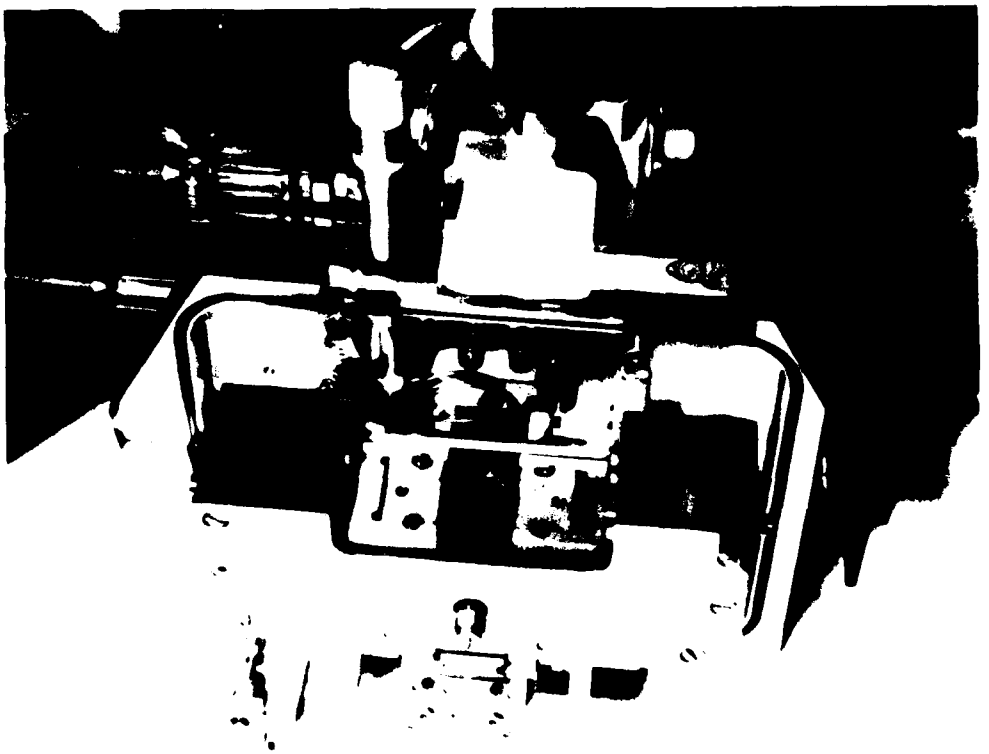

FIGURE 3. IN-SITU LOADING STAGE FOR SEM

polished to remove the EDM notch while leaving a small surface crack. Those samples which had been shot-peened were polished on both the front and back faces to prevent bowing. Micrographs of the resulting cracks are presented in Figures 4-8.

The d vs. $\sin^2\psi$ X-ray diffraction technique [4] was used to measure the residual stress level on all of the specimens. A computer program developed during the first year of this program was used to perform a second-degree curve fit to the intensity vs. 2θ data obtained from the X-ray stress measurements. Enough points are used to determine the peaks of interest at ψ = 15, 30, and 45°; then the peak positions and d spacings are calculated. The slope of d vs. $\sin^2\psi$ is obtained and used to calculate the residual stress. The coefficient of correlation for the linear curve fit is generally in the range of 97-99% indicating a high degree of accuracy in the measurements.

A 0.2° receiving slit and a 3° primary beam slit were used for all measurements. The 3° primary beam slit was masked with a 127 μm thick alpha brass foil to restrict the height of the beam impinging on the sample surface to within the thickness of the gage section. No Soller slits were used and the measurements for all peaks were performed with the detector at the focus position for each peak. Cr K_α radiation with a vanadium oxide filter was used in conjunction with the (211) plane for the steel specimens. The value of $E/(1+\nu)$ used for the steels was 1.59×10^5 MPa [5].

All testing was performed at room temperature. Prior to examination of the SCOD behavior, the samples were "shaken down" by several hundred cycles under load control in axial tension in the SEM stage. Load limits

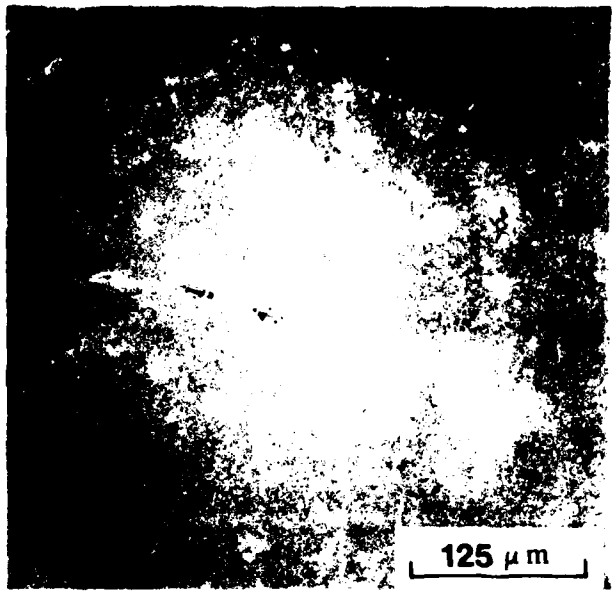

FIGURE 4. SURFACE MICROCRACK IN 4140 SPECIMEN 4140-1

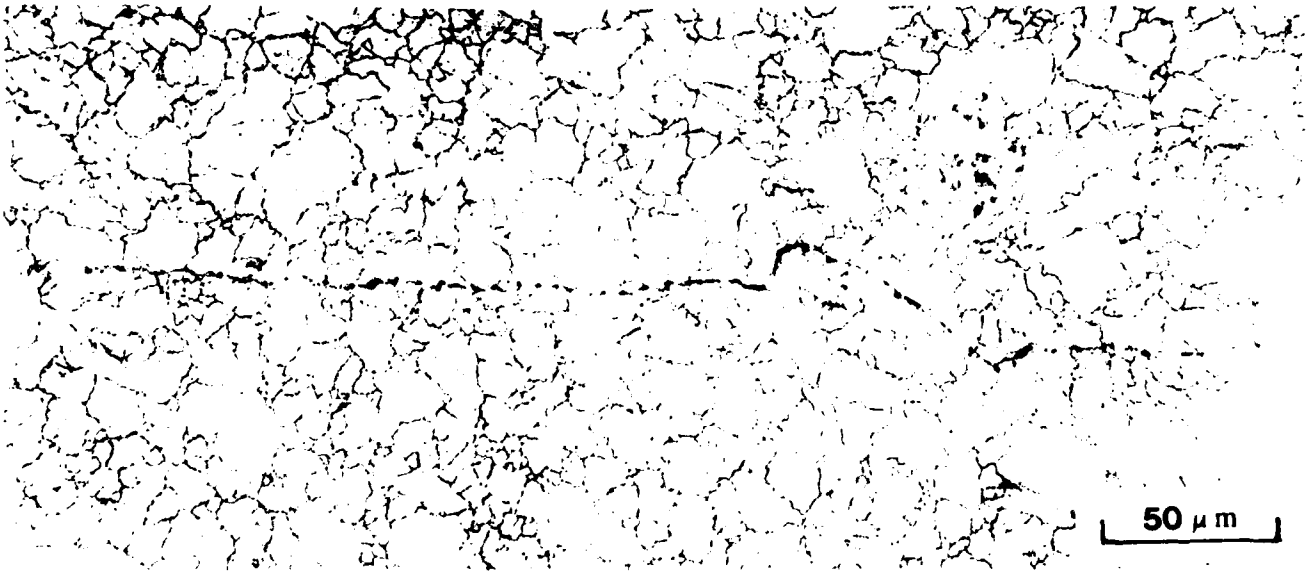

FIGURE 5. SURFACE MICROCRACK IN HY-130 SPECIMEN HY-8

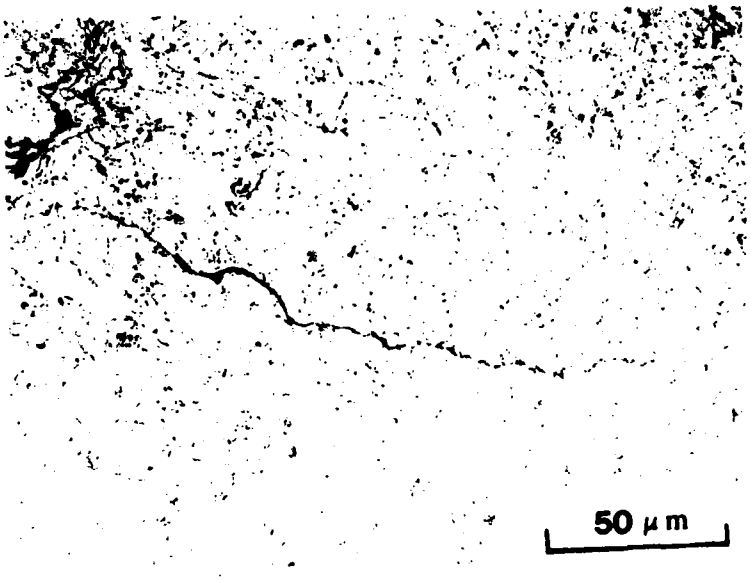

FIGURE 6. SURFACE MICROCRACK IN HY-130 SPECIMEN HY-9

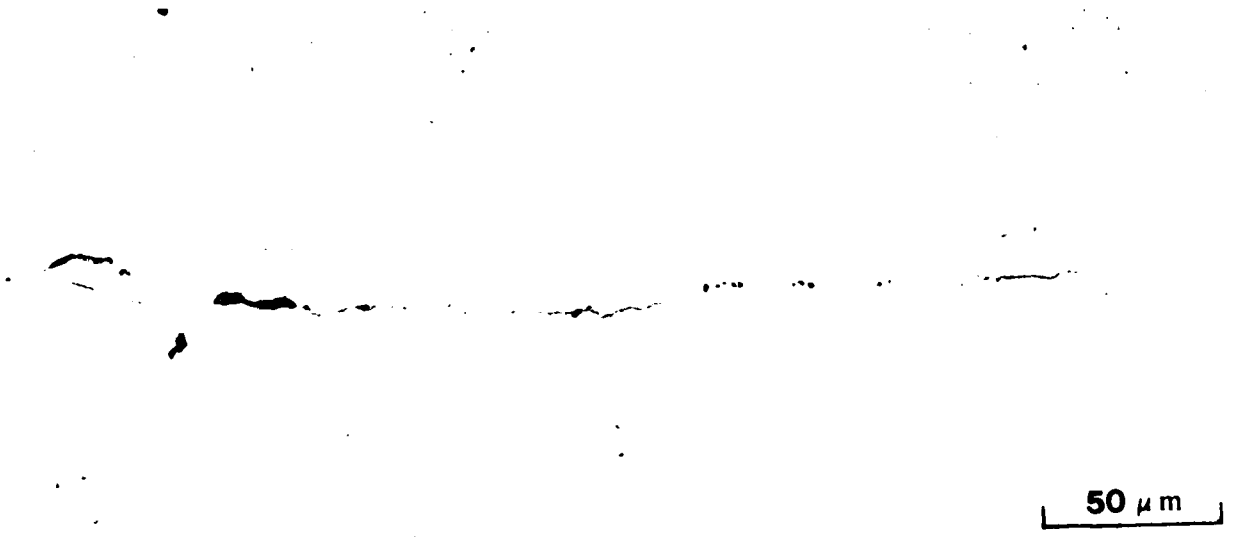

FIGURE 7. SURFACE MICROCRACK IN HY-130 SPECIMEN HY-11

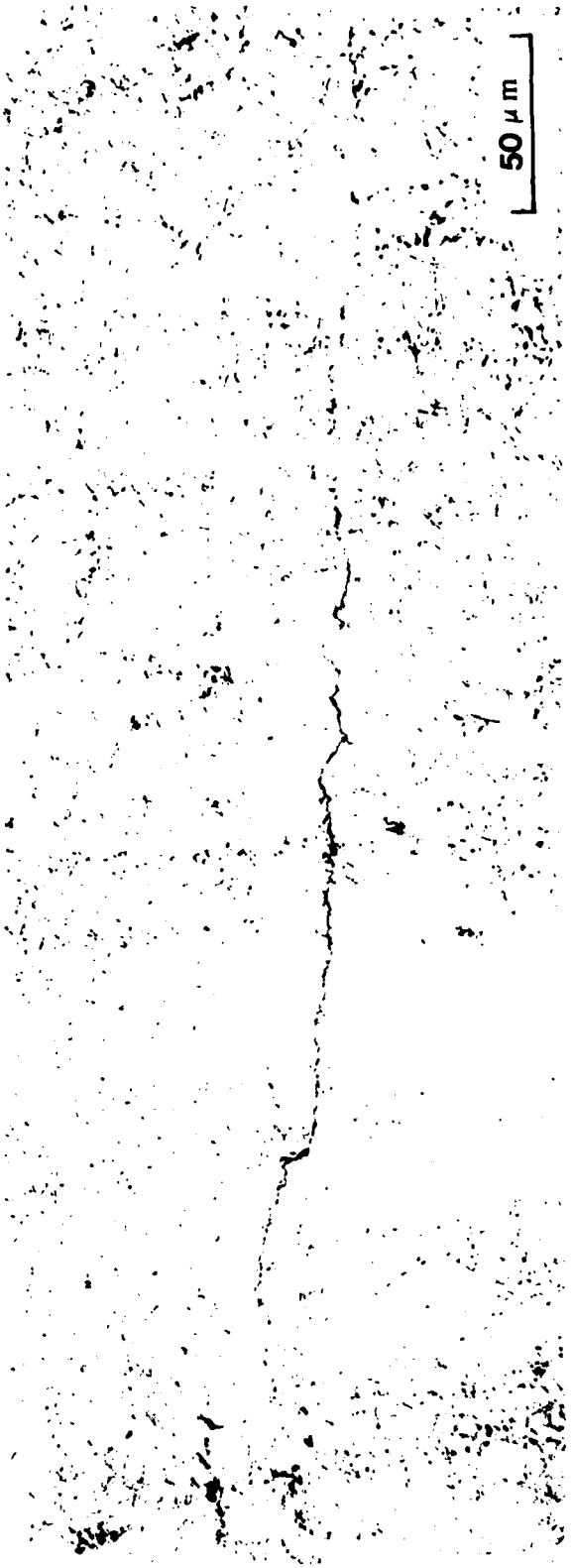

FIGURE 8. SURFACE MICROCRACK IN HY-130 SPECIMEN HY-14

used were ≈ 100 - 400 MPa for the 4140 and 100 - 600 MPa for the HY-130. Both static and dynamic measurements of the SCOD vs. load behavior were performed on the specimens. Dynamic observations were made at a cyclic frequency of 1 Hz. In addition, two specimens were cycled for 3000 - 4500 cycles in an aqueous solution of 3.5% NaCl after the initial measurements. SCOD vs. load behavior was remeasured for one of the specimens to determine the influence of the brine environment on crack opening. Measurements on the other specimen are currently being performed.

B. Results and Discussion

The uncorrected surface values of residual stress (σ_R) and surface crack lengths, as determined by optical metallography, for all specimens are compared in Table II. As can be seen from the data, surface crack length ranges from ≈ 175 - 500 μ. While the 4140 sample is virtually stress free, surface residual stresses in the HY-130 samples range from ≈ 160 - 660 MPa.

Micrographs and videotapes were taken at the center of the crack and at one of the crack tips at several loads for each specimen. The measured SCOD values as a function of applied stress are presented for the center of the crack for all specimens in Figures 9 and 10. In the case of the 4140 and the two HY-130 specimens with $\sigma_R \approx 160$ MPa, crack opening begins immediately with load and rises linearly throughout the experiment. The cracks in the two specimens of HY-130 with $\sigma_R \approx 660$ MPa did not open at all during the test.

This behavior can be compared with that found earlier for relatively large corner cracks in Ti-6Al-4V which had grown considerably below the depth of significant compression. Although described in more detail in

TABLE II

SAMPLE CHARACTERISTICS

Sample	Material	Surface Crack Length (μm)	Uncorrected Surface Residual Stress (MPa)
4140-1	4140	290	≈ 0
HY-8	HY-130	375	-640
HY-9	HY-130	175	-660
HY-11	HY-130	325	-165
HY-14	Hy-130	500	-165

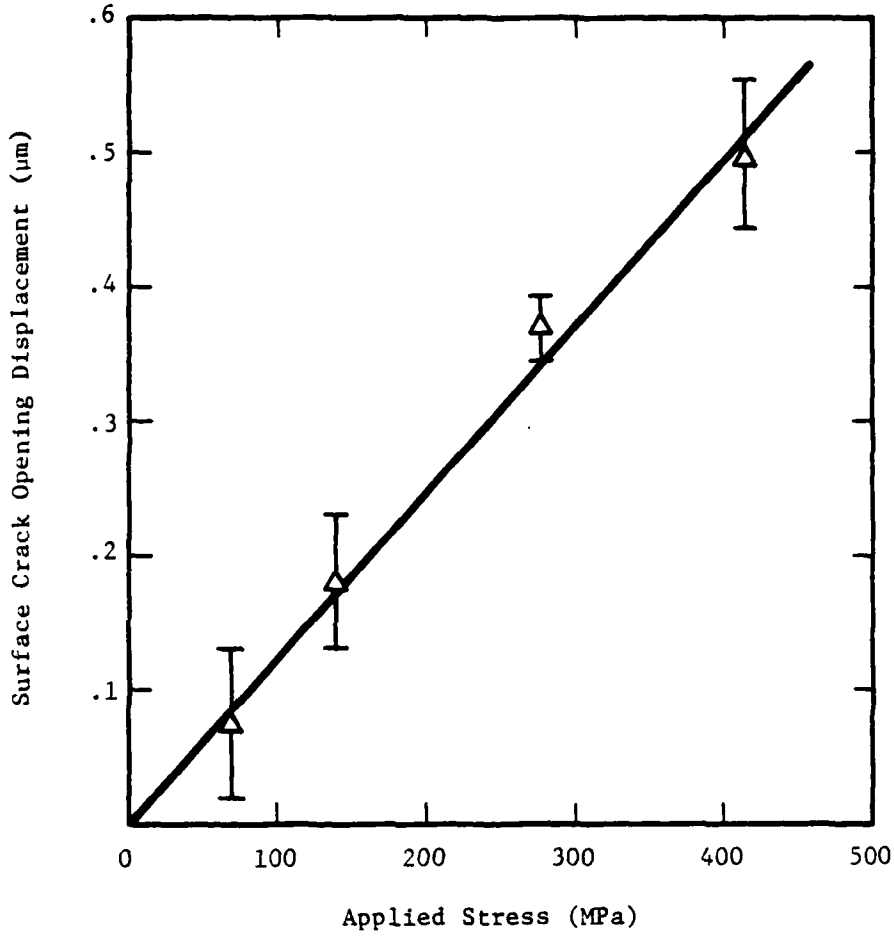

FIGURE 9. SURFACE CRACK OPENING DISPLACEMENT BEHAVIOR OF 4140 SPECIMEN 4140-1

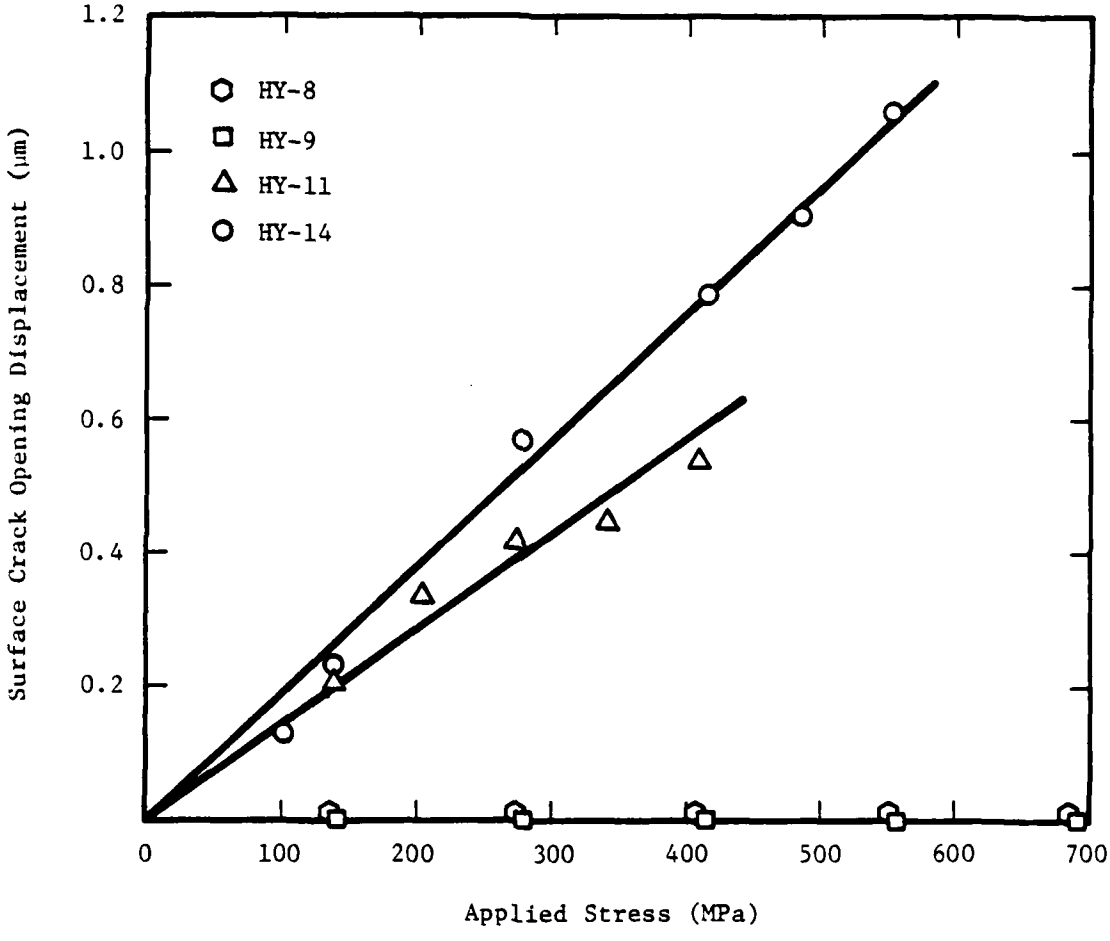

FIGURE 10. SURFACE CRACK OPENING DISPLACEMENT BEHAVIOR OF ALL HY-130 SPECIMENS TESTED IN AIR

the appendix, the main result of those experiments was that crack opening was delayed until the load increased to a value large enough to overcome the residual compressive stress due to peening. In the present case, it appears that the much smaller cracks in the steel specimens are completely within, or nearly so, the zone of residual compressive stress for the two specimens with $\sigma_R \approx 660$ MPa. When $\sigma_R \approx 160$ MPa, it does not appear to affect crack behavior significantly. Experience indicates that such a low value of compression is most likely extremely shallow and thus would not be expected to have a dramatic effect on crack opening. Profiles of the stress gradients in the HY-130 specimens are currently being performed to verify this point. Also, the two samples with $\sigma_R \approx 660$ MPa are being stress relieved so that the effect of the large residual compression can be verified.

The two samples of HY-130 which had $\sigma_R \approx 160$ MPa, HY-11 and HY-14, were cycled for 3000 cycles in air between the load limits 40 - 400 MPa. No apparent crack growth was detected on the surface of these specimens during the cycling. Cycling was then repeated in an aqueous solution of 3.5% NaCl. A plot of SCOD vs. load for HY-11 before and after the saltwater exposure is presented in Figure 11. As can be seen from the figure, the effect of the saltwater was to delay the opening of the crack until approximately 250 MPa. A comparison of crack opening in the two cases at a stress of 415 MPa is shown in Figure 12. Close examination of the crack surface after the saltwater exposure showed it to be filled with a corrosion product, presumably an oxide (Figure 13). Apparently the corrosion product wedged the crack open at some distance, thus preventing it from fully closing down during unloading. This is consistent with observations on

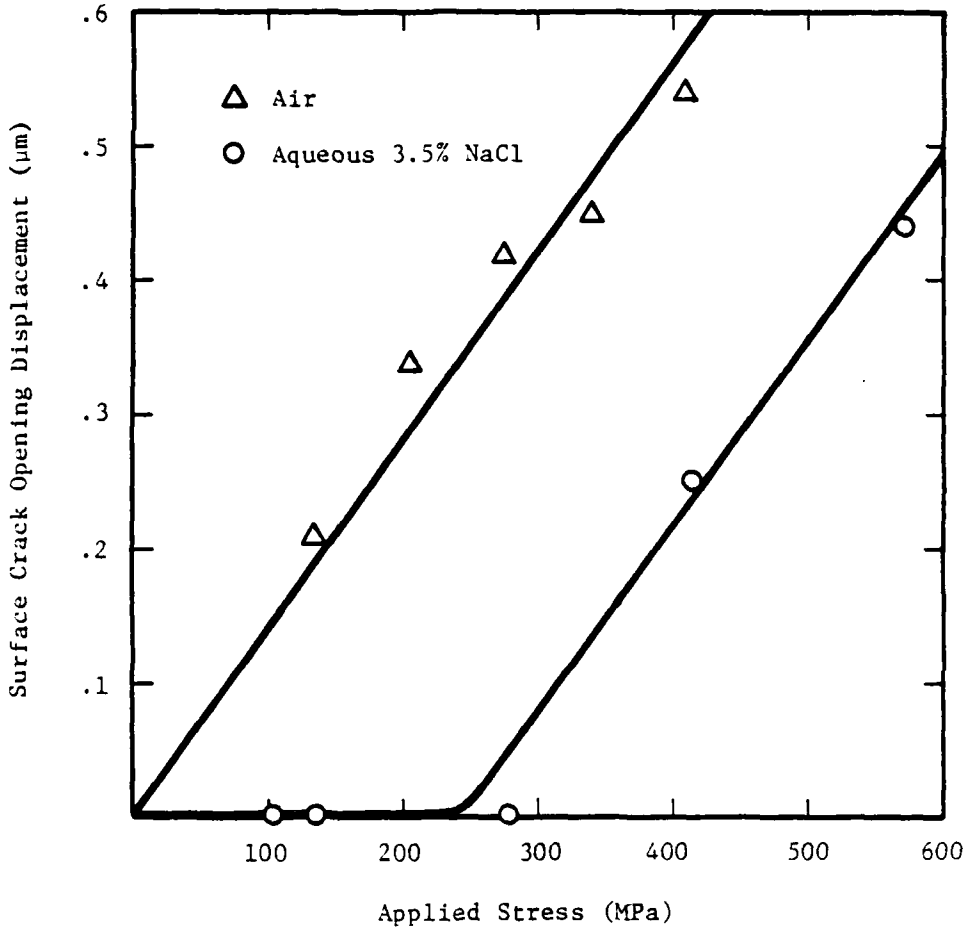

FIGURE 11. COMPARISON OF SURFACE CRACK OPENING DISPLACEMENT BEHAVIOR IN HY-130 SPECIMEN HY-11 IN AIR AND AN AQUEOUS 3.5% NaCl SOLUTION

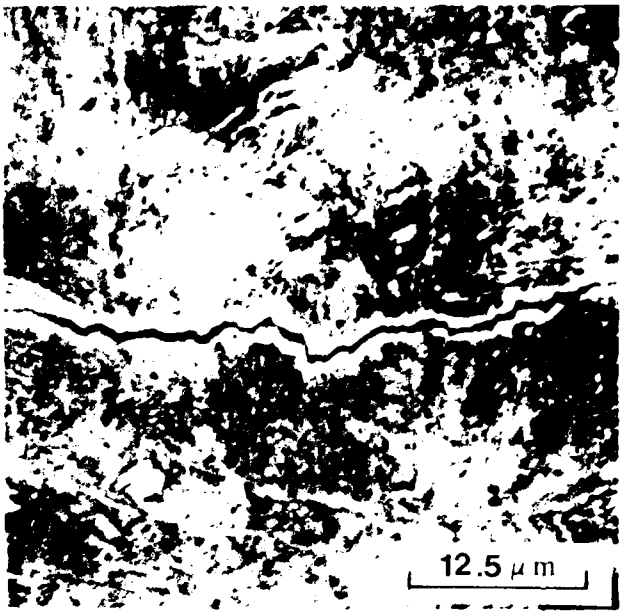

(a) Air Environment

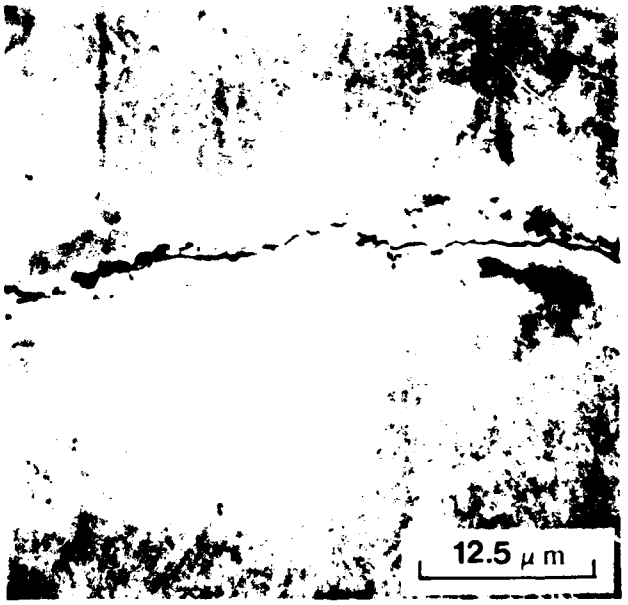

(b) Aqueous 3.5% NaCl Environment

FIGURE 12. COMPARISON OF SURFACE CRACK OPENING IN HY-130 SPECIMEN HY-11 IN AIR AND AN AQUEOUS 3.5% NaCl SOLUTION AT 415 MPa

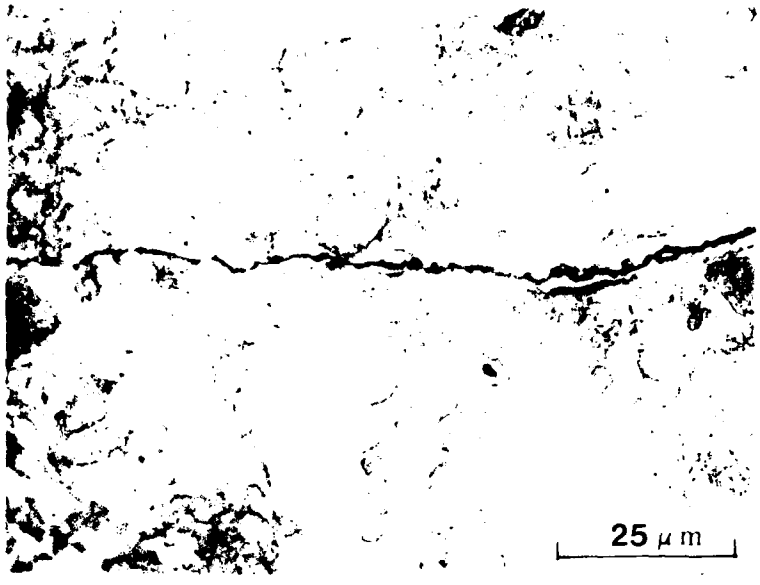

FIGURE 13. MICROGRAPH OF THE SURFACE MICROCRACK IN HY-130 SPECIMEN HY-11 AFTER CYCLING IN AN AQUEOUS 3.5% NaCl SOLUTION. Note that corrosion product fills the crack.

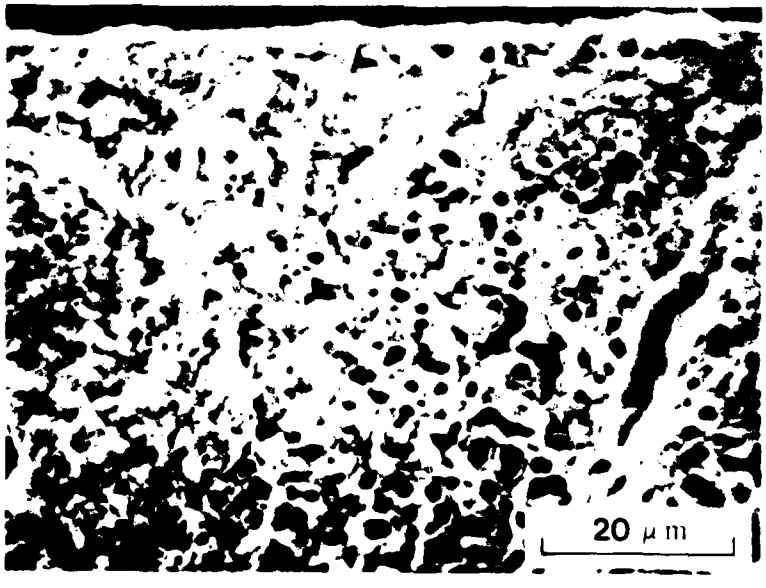

FIGURE 14. FRACTOGRAPH OF HY-130 SPECIMEN HY-11 AFTER CYCLING IN AN AQUEOUS 3.5% NaCl SOLUTION SHOWING SEVERE PITTING AND GENERAL CORROSION OF THE CRACK SURFACE

large cracks in HY-130 [6] and other steels [7] when growth is restricted to the near-threshold region. This wedging action of the corrosion product effectively reduces the applied ΔK; thus, it reduces crack growth.

Sample HY-11 was subsequently broken open to reveal the internal crack surfaces. Figure 14 shows the severe pitting and oxidation which was typical of the entire crack surface in this specimen. Similar measurements are currently being performed on Sample HY-14. An attempt will be made to profile the crack in this case to determine the amount of wedging at the buried crack tip.

III. PREDICTION OF SCOD VS. LOAD BEHAVIOR

A. Comparison of Predicted and Observed Surface Microcrack Openings

A detailed description of the analytical approach developed for the prediction of SCOD behavior in surface cracks and a summary of previous results are given in the appendix. In general, it was found that the approach gave excellent correlation between predicted and observed SCOD behavior for Mode I surface microcracks, corner cracks, and surface microcracks when no surface residual stresses were present. The presence of a residual compressive stress gradient produced an overestimation of crack opening with load. This problem will be dealt with in Part B of this section.

Prior to this report, comparison of experimental and predicted results has only been reported for Ti-6Al-4V. During the current year, comparisons between predicted and observed openings were performed for the 4140 specimen. The results of the comparison are presented in Figure 15. Again, excellent agreement was obtained between prediction and experiment (recall that the 4140 specimen was stress free). The large error bars are due to the extremely small openings in the 210 GPa modulus steel. (The modulus for Ti-6Al-4V is about one-half that for steel.) Accuracy in such measurements can be improved by viewing the videotapes on a wide screen, projection-type television. Dynamic measurements on the steel specimens discussed in this report are currently beind conducted. These data will be used for similar comparisons for the two HY-130 specimens in which opening was observed.

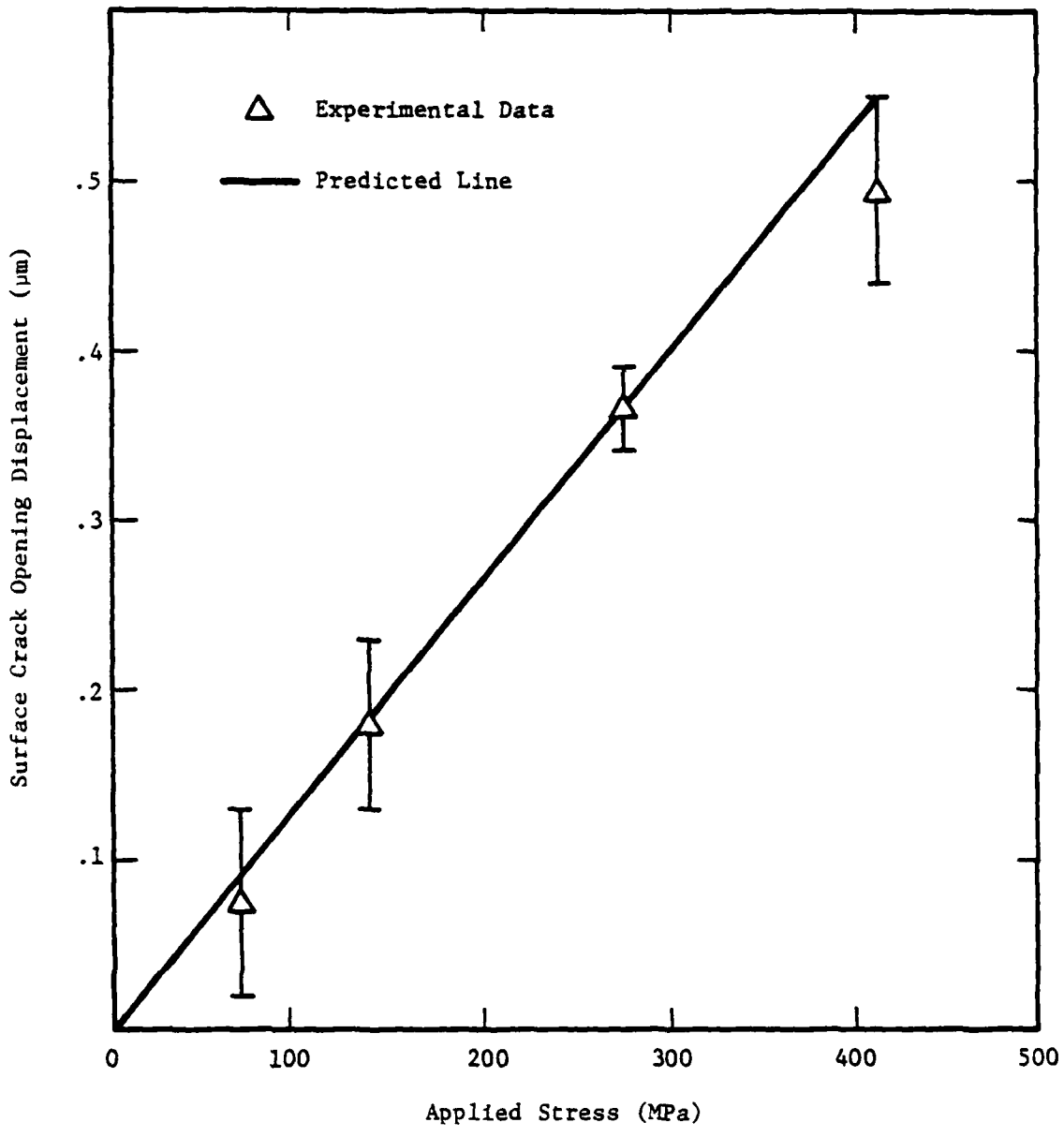

FIGURE 15. COMPARISON OF OBSERVED AND PREDICTED SURFACE CRACK OPENING DISPLACEMENT BEHAVIOR OF THE SURFACE MICRO-CRACK IN 4140 SPECIMEN 4140-1

B. Prediction of SCOD Behavior in the Presence of a Residual Stress Gradient

As mentioned above, the results included in the appendix show that the analytical approach used in this program overpredicts crack opening with load when a near-surface residual compressive stress gradient is present. The approach is based on combining an expression for the displacement of a part-through crack due to Irwin [8] with values of the surface crack tip stress intensity factor obtained from a computer program called BIGIF (Boundary Integral Generated Influence Functions) [9]. The BIGIF program calculates a "global" stress intensity factor for each position by integrating over the crack front. Thus, the constraints introduced by a three-dimensional part-through crack and an imposed gradient in stress across the crack are readily handled. Theoretically then, the stress intensity factors calculated by BIGIF should be appropriate.

The logical source of the discrepancy lies in the opening expression itself. The opening expression derived in the appendix assumes that the crack opens as a semiellipse. Thus, the crack profile is constrained to follow a prescribed elliptical path for a given loading condition and crack geometry. If the applied stress is not uniform, as in the case of the near-surface residual compressive stress gradient imposed on the corner cracks in Ti-6Al-4V described in the appendix, the results indicate that the crack can close down more at the surface than at some point underneath the surface. This is due to the fact that the buried crack tip, if it has grown out of the region of significant residual stress, is only influenced by the residual stress gradient insofar as it is connected to the

surface by the material along the crack front. In this instance, the buried crack tip will open to a significant fraction of the elastic opening which it would have had if no residual stress gradient were present. The result will be a lenticular crack profile through the thickness which violates the geometry of the SCOD derivation.

In order to account for this discrepancy, another computer program (3D-BINTEQ; 3-D Boundary Integral Technique) [10] has been obtained which allows the direct calculation of crack surface displacements in the presence of residual stresses. This program also uses the boundary integral technique and served as the basis for the derivation of the influence functions for the various crack geometry options available in BIGIF. This relationship assures compatibility between stress intensity factor and crack opening displacement results. An appropriate elemental model for the corner cracks described in the appendix has been formulated and runs are currently being made to assess the success of predictions of SCOD for these cracks in the presence of residual stresses.

C. Lifetime Predictions for Cracks Under the Influence of Surface Residual Stresses

The overall objective of this program is to be able to predict how residual stresses and environment affect crack growth behavior and, thus, component lifetime. Another reason for choosing BIGIF for use in this program was the inherent ability to compare calculated stress intensity data with tabulated crack growth data. The version of BIGIF used herein also has the ability to incorporate negative R-ratio effects with the equation derived by Yuen et al [11]. This allows the superposition of residual compressive stress gradients.

Using the crack geometry in Figure 16 and the residual stress gradient from Sample Ti-2 (see appendix) shown in Figure 17, parametric lifetime runs were calculated for a Ti-6Al-4V sample with a surface microcrack at the center of one of its faces. A K_{Ic} value of 65 MPa$\sqrt{m}$ was used for the purposes of the calculation. Two a/c ratios were used, 0.2 and 0.6, with three crack depths. The smallest crack depth represented the buried tip resting at the point of maximum residual compression; the intermediate crack depth represented the buried tip resting at the boundary of the zone of significant residual compression; and the largest crack depth represented the buried crack tip resting well outside of the zone of residual stress.

A comparison of lifetime results for the cases of no residual stresses present vs. the cases with the residual stress gradient of Figure 17 is presented in Table III. As can be seen from the data, a slight increase in lifetime is obtained in the sample which has a near-surface residual stress gradient when the crack depth is either at the boundary of significant residual compression or when the crack depth is well past the boundary. When the crack is completely imbedded in the zone of residual compression, however, an order of magnitude increase in lifetime is found. Thus, the residual stress gradient dramatically affects the initial stages of crack growth.

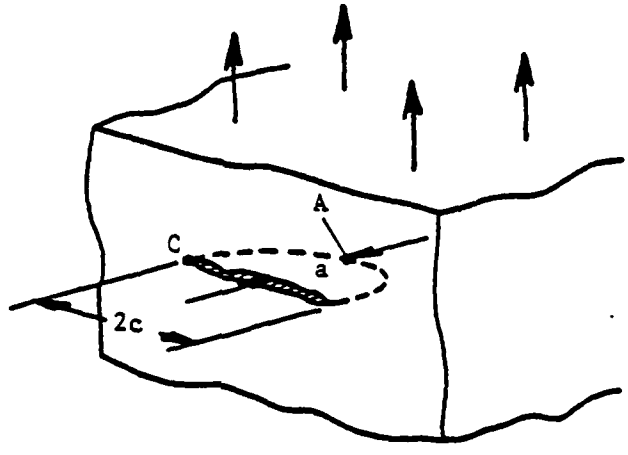

FIGURE 16. CRACK GEOMETRY USED IN ANALYTICAL APPROACH

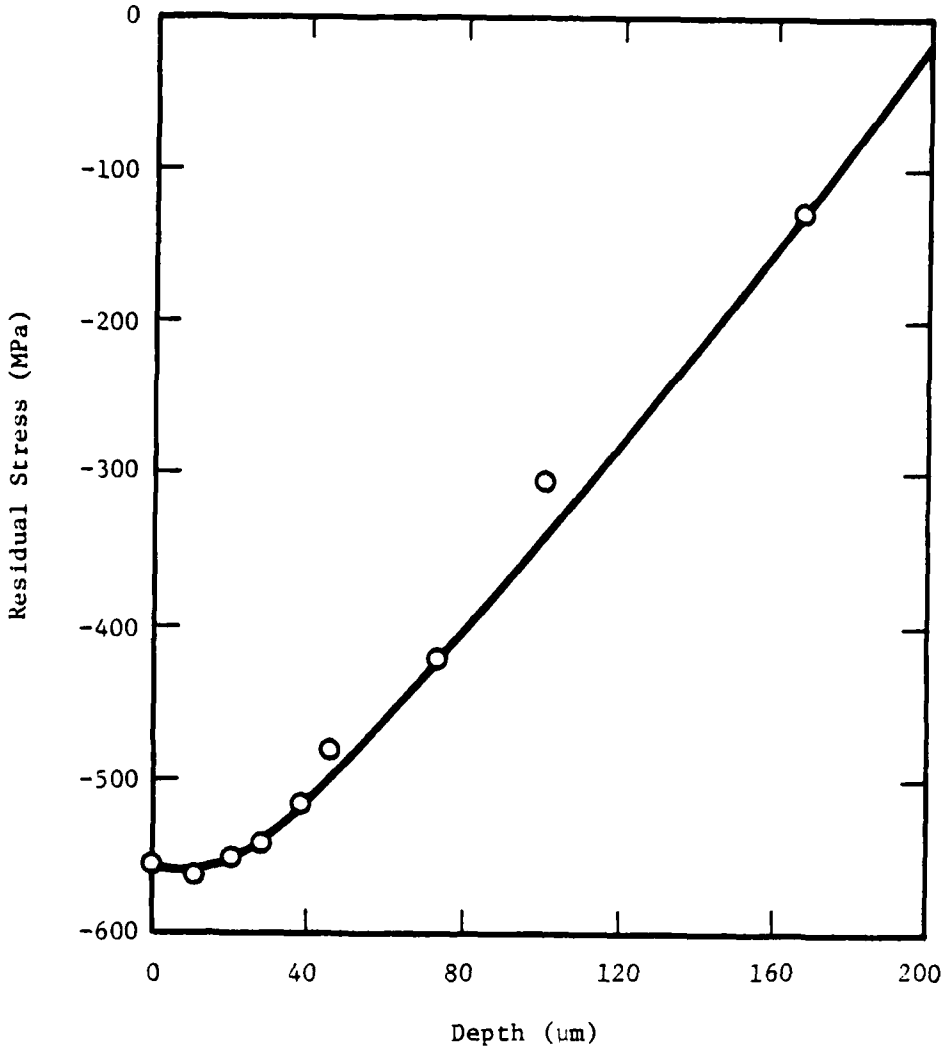

FIGURE 17. NEAR-SURFACE RESIDUAL STRESS GRADIENT USED IN BIGIF PARAMETRIC RUNS

TABLE III

COMPARISON OF LIFETIME PREDICTIONS FROM PARAMETRIC BIGIF CALCULATIONS FOR THE EFFECT OF NEAR-SURFACE RESIDUAL STRESS GRADIENTS

Crack Depth (μm)	a/c	Compressive Residual Stress Gradient Present	Cycles to Failure
635	0.2	No	1,387
		Yes	1,508
635	0.6	No	2,331
		Yes	2,583
216	0.2	No	3,211
		Yes	4,236
216	0.6	No	4,615
		Yes	6,622
22	0.2	No	13,383
		Yes	103,170
22	0.6	No	19,262
		Yes	187,190

IV. CONCLUSIONS

1. A 3.5% NaCl aqueous environment significantly affects the SCOD, thus growth behavior, of surface microcracks in HY-130. Oxide wedging of a microcrack in this region, where the oxide thickness is on the order of the SCOD, appears to reduce the effective ΔK on the crack. A reduction in crack growth rate is expected due to this phenomenon.
2. The analytical approach previously developed on this program accurately predicts crack opening vs. load for steels as well as Ti alloys in the absence of near-surface residual stress gradients.
3. The inability of the analytical approach to properly predict SCOD behavior when a near-surface residual stress gradient is present is most likely due to a violation in the assumptions inherent in the opening expression. The use of a boundary integral computer program should allow for proper calculation of opening behavior.
4. Crack growth calculations show that residual compressive stress gradients (such as those obtained by shot-peening) can have a dramatic effect on the lifetime of surface flaws when the cracks are completely imbedded in the stress field. A slight advantage in lifetime is still maintained even if the crack is deeper than the zone of significant residual stress.

V. REFERENCES

1. A. J. McEvily and T. L. Johnston, Int. J. Frac. Mech., vol. 3, 1967, p. 45.

2. G. G. Garrett and J. F. Knott, Met. Trans., vol. 7A, 1976, p. 884.

3. D. L. Davidson and A. Nagy, J. Phys. E. (Sci. Inst.), vol. 11, 1978, p. 207.

4. E. Macherauch, Exp. Mech., vol. 6, 1966, p. 140.

5. A. L. Christenson and E. S. Rowland, Transactions of the ASM, vol. 45, 1953, p. 638.

6. S. J. Hudak, Jr., unpublished research, Southwest Research Institute, San Antonio, TX, 1981.

7. S. Suresh, G. F. Zamiski, and R. O. Ritchie, Met. Trans., vol. 12A, 1981, p. 1435.

8. G. R. Irwin, J. Appl. Mech., December 1962, p. 651.

9. P. M. Besuner, D. C. Peters, and R. C. Cippola, BIGIF Fracture Mechanics Code for Structures, Key Phase Report, NP-838 Research Project 700-1, EPRI, July 1978.

10. T. A. Cruse, An Improved Boundary-Integral Equation Method for Three-Dimensional Elastic Stress Analysis, Interim Report on Contract DA-ARO-D-31-124-72-G3, Carnegie-Mellon University, August 1973.

11. A. Yuen, S. W. Hopkins, G. R. Leverant, and C. A. Rau, Met. Trans., 1974, vol. 5, p. 1833.

VI. PUBLICATIONS AND PRESENTATIONS

A. Publications

1. J. E. Hack and G. R. Leverant, "On the Prediction of the Surface Crack Opening Displacement of a Part-Through Crack," International Journal of Fracture, vol. 16, pp. R15-18, 1980.

2. J. E. Hack and G. R. Leverant, "The Influence of Compressive Residual Stress on the Crack Opening Behavior of Part-Through Fatigue Cracks," accepted for publication in an ASTM Special Technical Publication on Residual Stress Effects in Fatigue, 1981.

B. Presentations

1. "Real-Time Observation of the Behavior of Fatigue Microcracks Residing in Surface Residual Stress Fields in Ti-6Al-4V" by J. E Hack and G. R. Leverant, presented at the 109th AIME Annual Meeting, February 1980, Las Vegas, Nevada.

2. "The Effect of Surface Residual Stresses on the Crack Opening Displacement of Surface Fatigue Cracks" by J. E. Hack and G. R. Leverant, presented at the 110th AIME Annual Meeting, February 1981, Chicago, Illinois.

3. "The Influence of Compressive Residual Stress on the Crack Opening Behavior of Part-Through Fatigue Cracks" by J. E. Hack and G. R. Leverant, presented at the ASTM Symposium on Residual Stress Effects in Fatigue, May 11, 1981, Phoenix, Arizona.

APPENDIX

THE INFLUENCE OF COMPRESSIVE RESIDUAL STRESS ON THE CRACK OPENING BEHAVIOR OF PART-THROUGH FATIGUE CRACKS

by

J. E. Hack[1] and G. R. Leverant[1]

Presented at

Symposium on Residual Stress Effects in Fatigue
Phoenix, Arizona
May 11, 1981

---

[1] Research Metallurgist and Manager, respectively, Metallurgy Section, Southwest Research Institute, 6220 Culebra Road, San Antonio, TX 78284.

ABSTRACT: Direct observations of the surface crack opening displacement (SCOD) of surface and corner fatigue cracks were made on samples of Ti-6Al-4V under both cyclic and static loading conditions. The experiments were conducted in-situ in a scanning electron microscope. Results show that surface residual stresses can significantly affect crack opening behavior, thus crack growth behavior, even when the crack has grown well beyond the zone of residual stress. An analytical approach was developed and used to predict SCOD for Mode I part-through cracks based on crack geometry and the boundary integral technique. Correlation with independent results for macrocracks and values for microcracks measured in this program are excellent for the case of zero residual stress. The analytical approach is currently being extended to more accurately account for the presence of residual stress gradients.

KEY WORDS: residual stress, fatigue, part-through crack, crack opening displacement, stress intensity, titanium.

Residual stresses are introduced in metal surfaces by many common mechanical and thermal processes. Their introduction can be intentional, as in the case of shot-peening, or inadvertent, as in the case of differential contraction between weld metal and base material during solidification and cooldown. The affected region due to shot-peening is generally quite thin with a maximum depth of 125-250 μ, while welding-induced residual stresses can extend to significant depths in the material. Since fatigue crack initiation usually occurs at or near a free surface and initial growth rates are very low (≈ 10^{-6} mm/cycle), fatigue cracks spend a significant portion of their lifetimes under the influence of the surface residual stress state. Although several studies [1-3] have been conducted to evaluate the effects of surface condition on fatigue behavior in both ferrous and nonferrous alloys, the fundamental relationship between surface condition and fatigue crack initiation and growth remains to be defined.

Data by Leverant et al [4] and others [5] have shown that surface residual stresses do not significantly alter crack initiation behavior in titanium alloys but that crack propagation can be profoundly affected by their presence. This suggests that residual stresses act to modify crack opening displacement (COD) behavior by changing the effective stress intensity range [$COD \simeq \Delta K^2_{eff}/(4E\sigma_y^2)$]. Since COD can be directly related to crack growth [6,7], the surface residual stress state could markedly affect propagation behavior without necessarily influencing the number of cycles required for Stage I crack initiation.

The present investigation was undertaken to quantify the effects of surface residual stresses on surface crack opening displacement (SCOD)

behavior of part-through cracks. In the context of this paper, SCOD is defined as the crack opening at the central portion of the crack as opposed to the opening at the tip of the crack. Current results of experimental observations are presented herein which compare SCOD behavior in the absence and presence of a compressive residual stress field. In addition, the initial results of attempts to analytically model SCOD vs. load behavior are presented.

MATERIAL AND EXPERIMENTAL PROCEDURES

The chemical analysis of the Ti-6Al-4V material used in this study is given in Table 1. The material was machined from a pancake forging that was forged at 1241 K in the alpha-beta phase field, annealed for one hour at 1227 K, water quenched and then aged at 977 K for two hours. This resulted in a microstructure of primary alpha embedded in a matrix of transformed beta with an average alpha particle size of approximately 14 μm. The microstructure is shown in Figure 1.

A cantilever beam fatigue specimen was designed to ensure surface crack initiation. Figure 2 shows the tapered gage section which yields a constant stress over the entire gage length. It can be seen from the figure that slots are incorporated in the grip sections to allow for fixturing the specimen into the SEM loading stage after the initation of cracks in a bending rig.

The SEM loading stage is shown in Figure 3. The stage is capable of cyclically loading a sample in tension-tension at loads up to 3780 Newtons at frequencies ranging from 0-5 Hz while maintaining the area of interest within the viewing screen of the SEM and in focus. Crack behavior can be videotaped and replayed for analysis of crack opening displacement response. In addition, samples can be statically loaded in tension at loads up to 4895 Newtons.

Residual stress was introduced in the specimen surfaces by shot-peening at an intensity of 0.011A. The samples were then lightly polished by standard metallographic techniques. A final electropolish and light etch (85 H_2O - 10 HF - 5 HNO_3) were then used to reveal the surface microstructure of the specimens. A total of less than 75 μm of material was removed by this process which allowed the elimination of the surface roughness induced by the peening without significant relaxation of the surface residual stress state. Material was removed equally from both sides of the specimen to prevent specimen bowing.

The two-exposure x-ray technique [8] was used to measure the surface residual stress on all the samples. A computer program was developed to perform a parabolic curve fit on the intensity vs. 2θ data obtained from the x-ray measurements. Enough points were used to define the peaks of interest at $\psi = 0$ and 45°, then the peak positions, peak shift, and residual stress were calculated. A comparison of measurements on a sample with a slight amount of compressive residual stress taken at different times under similar conditions showed that the technique was reproducible to within ± 0.015° for peak positions and ± 5.06 MPa in residual stress (Table 2). This is well within the predicted accuracy of the technique [8].

Cu K_α radiation was used for all measurements in conjunction with a 0.2° receiving slit and a 3° primary beam slit. The 3° primary beam slit was masked with a 127 μm thick alpha brass foil to restrict the height of the beam impinging on the sample surface to within the thickness of the gage section. No Soller slits were used and the measurements for all peaks were performed with the detector at the focus position for each peak. A Ni filter was used to ensure a strong Cu K_α peak. The (213) plane of alpha titanium was chosen for the diffracting plane which has

a peak at approximately $2\theta = 141°$. The stress constant for these conditions is 5.51 MPa/0.01° $\Delta 2\theta$.

Residual stress profiles were obtained by alternating x-ray stress measurements and removal of material by electropolishing until the stress became negligible. Profiles were corrected for both beam penetration and stress relaxation due to layer removal.

All samples were precracked in bending within the strain limits of 0.3 ± 0.5% at 1 Hz. All testing was performed at room temperature. Prior to examination of the SCOD behavior, the samples were "shaken down" by several hundred cycles under load control in axial tension in the SEM loading stage. Load limits used for the shakedown were 100-560 MPa applied at 1 Hz. Both static and dynamic measurements of the SCOD vs. load behavior were performed on the three specimens.

Dynamic observations of the cyclic loading were videotaped for real time measurement of SCOD. The samples were also step loaded to allow for still photographs at each loading increment. SCOD vs. load data obtained by these two techniques were compared for consistency. One sample, Ti-6, was stress-relieved subsequent to the initial SCOD measurements and the measurements were then repeated. This allowed a direct observation of the effect of residual stress on crack opening for a particular crack. After all testing was completed, crack geometries were obtained by incremental polishing through the specimen with measurements of crack length taken at each depth.

RESULTS AND DISCUSSION

Experimental

The corrected compressive portions of the residual stress profiles for Samples Ti-2 and Ti-6 are presented in Figure 4. The profile for

Ti-6 was determined on a separate specimen which underwent similar treatment and had a comparable surface stress value in order to allow for stress relief of Ti-6 after the initial SCOD measurements. As can be seen from the data, the two specimens differ in maximum compressive residual stress by approximately 300 MPa, although both samples have a significant amount of compression at their surfaces.

The cracks used for observation in both Ti-2 and Ti-6 were corner cracks with profiles, as shown in Figure 5. It should be noted that the shaded portion represents the extent of the zone of compressive residual stress. The effects of balancing tensile stresses were ignored due to the fact that they act over a much larger area and will not attain a significant magnitude. Thus, most of the crack front in both specimens had grown well out of the zone of significant residual stress prior to the SCOD measurements.

At several loads, crack opening was recorded by micrographs and videotape at the center of the crack and at the crack tip on the polished face of each specimen. The measured SCOD values as a function of applied stress are presented for the center of the crack in Figure 6. Since dynamic and static measurements were extremely close in value, average values were used to draw the graphs. Any effects of residual opening have been subtracted out. In both cases, the crack remains closed until the stress reaches approximately 300 MPa. After that point, the SCOD increases approximately linearly with stress. This is illustrated in the sequence of photographs from Sample Ti-6 in Figure 7.

Figure 8 shows the crack tips away from the edge in both samples at maximum load. As can be seen from the figures, the tips have only just

begun to open, even at loads approaching 560 MPa. This indicates that the residual compressive stress present at the surface of the two specimens is strongly influencing the surface crack tip opening displacement (CTOD) through the entire loading cycle.

Figure 9 presents a comparison of the SCOD vs. load behavior of Sample Ti-6 before and fter a stress relief heat treatment conducted at 540°C for one hour in vacuum. As can be seen from the figure, subsequent to the stress relief treatment, crack opening begins shortly after the application of load. In addition, the opening increases linearly with stress as soon as the crack begins to open.

Above a stress of approximately 350 MPa, the SCOD vs. stress curve for the stress-relieved material becomes nonlinear. This behavior indicates a plastic yawing open of the crack tip. Such opening is apparent in the sequence of photographs in Figure 10 which contrast the surface CTOD in Sample Ti-6 at two loads before and after the stress relief treatment. The photographs show that while the crack tip in Ti-6 in the shot-peened condition remains closed (or nearly so) throughout the entire loading sequence, the crack tip in the stress-relieved condition begins to open with the onset of nonlinearity in the SCOD vs. load curve (Figure 9). In addition, while no growth occurred during the experiments performed on the two samples in the shot-peened condition, Figure 10 shows that the crack in Ti-6 did propagate across several grains ($\simeq$ 40 μ) during the course of the experiment after the stress relief treatment. This crack growth can actually be observed in the videotaped sequences. These results emphasize the strong influence that the surface stresses have on surface crack opening, and thus crack growth, behavior. Even

after the majority of the crack has moved out of the residual stress field, the surface opening is still reduced substantially by the compressive surface stress state and, consequently, surface crack growth is reduced. This observation has strong implications with respect to approaches being proposed for component removal from service (e.g., retirement-for-cause) based on nondestructive inspection and fracture mechanics.

Analytical Prediction of SCOD Behavior

Concurrent with the experimental observations described in the previous section, the development of an analytical approach was initiated to allow for the prediction of SCOD behavior under the influence of residual stress. The approach chosen is based on the stress intensity at the surface crack tip. A general expression for the SCOD of an elliptical crack was derived from the work of Irwin [9] which gives:

$$SCOD(r) = 2\eta = 2\eta_o \frac{\sqrt{r}}{ac}\left[2ac\left(a^2\cos^2\phi + c^2\sin^2\phi\right)^{1/2} - r\left(a^2\cos^2\phi + c^2\sin^2\phi\right)\right]^{1/2}$$

where η is the half crack opening at the point of interest, and r, η_o, a, c, and ϕ are as defined in Figures 11 and 12. Thus, at $\phi = 0$ and $r = c$ it is found that the SCOD of a surface crack is simply:

$$SCOD = 2\eta = 2\eta_o \quad .$$

For the case of the corner cracks studied, where $\phi = 0$ and $r = c/2$,

$$SCOD = 2\eta = \sqrt{3}\,\eta_o \quad .$$

In these expressions,

$$\eta_o = \frac{2(1 - \nu^2)\ \sigma a \left[1 + .12\left(1 - \frac{a}{c}\right)\right]^*}{E\,\Phi}$$

where ν = Poisson's ratio of the material

σ = Applied stress

E = Young's modulus of the material

Φ = Elliptic integral of the second kind

$$\left(\int_0^{\pi/2}\left[1 - \left(1 - \left[\frac{a}{c}\right]^2\right)\sin^2\phi\right]^{1/2} d\phi\right)$$

Recognizing that the stress intensity at the surface, K_s, is given by:

$$K_s = \frac{\sigma}{\Phi}\sqrt{\pi a}\sqrt{\frac{a}{c}}\left[1 + .12\left(1 - \frac{a}{c}\right)\right]^*$$

then

$$\eta_o = \frac{2\,(1 - \nu^2)\,\sqrt{c}\,K_s}{\sqrt{\pi}\,E}$$

It was desired to maintain complete generality in the analytical approach so that the contributions of a residual stress field could be incorporated for both corner and surface cracks. Consistency among these various cases was attained by obtaining values of K_s from a computer program known as BIGIF [11]. This program calculates values for K_s by the boundary integral technique [12] and is capable of treating the geometry and stress states studied in this program.

---

* Another free surface correction must be made for corner cracks, so the term in brackets must be made to read [1 + .2 (1 - a/c)] in this case [10].

As can be seen from the equations, SCOD behavior for a given material is dependent on the surface crack tip stress intensity and the surface crack length. Predictions based on these expressions were compared to independent data on macro surface cracks in Ti-6Al-4V of equivalent microstructure and yield strength gathered by Collipriest [13]. In his work, Collipriest initiated surface cracks in samples and measured SCOD vs. load until the behavior became extremely nonlinear (i.e., gross plasticity and extension of the crack). Then he fatigued the sample for a short time to mark the end of the first crack extension and repeated his measurements. Figure 13 shows a comparison of SCOD as calculated in the present study to that measured by Collipriest on a 10,000-μm long surface crack. As can be seen from the figure, the agreement is excellent up to the point where the measured behavior becomes nonlinear.

The applicability of this analytical approach to micro surface cracks was subsequently investigated. Figures 14(a) and (b) show 50- and 32-μm long surface cracks, respectively, in a sample which has been surface ground parallel to the stress axis. The a/c ratios of the 50- and 32-μm cracks were 0.45 and 0.70, respectively. Little or no surface residual stress was present in this specimen. Figure 15 shows a comparison of measured versus predicted behavior for these two cracks. As can be seen from the figure, the results of the calculations again give excellent correlation with the experimental observations. It should be mentioned that one would not normally expect linear elastic fracture mechanics to apply when the crack length and depth are on the order of the grain size of the material. It is believed that the extensive degree of cold work in the ground surface causes the near surface material,

in which the crack is wholly contained, to act as a continuum. Indeed, experimental results obtained on 7 to 18-μm long surface cracks in an electropolished surface of Ti-6Al-4V do not agree with predictions based on the present analytical approach [14].

This analytical approach was also evaluated for the experimental data on the two corner cracks which were under the influence of a large compressive residual stress. Comparisons of SCOD at maximum load are given in Table 3. The previously determined residual stress profiles were accounted for where applicable. As can be seen from the data, the correlation between predicted values and experimental values is excellent for the stress relieved case. When a compressive residual stress field is present, the predicted openings are larger than those actually observed.

The source of the latter discrepancy can either be a result of an overestimation of K_s in BIGIF or the failure of the opening expression when a stress gradient is present. In an attempt to resolve this anomaly, another computer program based on the boundary integral technique, 3-D BINTEQ [15], is currently being used to calculate SCOD directly. These results will then be compared to those obtained through the combination of BIGIF and the derived crack opening expression.

CONCLUSIONS

1. It has been demonstrated that surface residual stresses exert a significant influence on the surface crack opening displacement (and, therefore, effective stress intensity) of part-through fatigue cracks in Ti-6Al-4V, even if the majority of the crack front resides outside the zone of residual stress.

2. An analytical approach has been developed for predicting the surface crack opening displacement (SCOD) of part-through Mode I cracks. It has been applied to macrocracks as well as microcracks as small as 20 to 25 μm in depth.

3. In the absence of residual stress, agreement between calculated and measured SCOD is excellent. In the presence of a high level of residual surface compressive stress, the predicted SCOD is somewhat larger than the measured value.

4. The closure of surface cracks due to high compressive stresses may have a significant impact on the ability to detect these cracks by conventional nondestructive inspection methods. This could have significant implications with respect to run/retire decisions for critical components.

ACKNOWLEDGEMENTS

The authors are grateful for the support of the Office of Naval Research under Contract N00014-78-C-0674.

REFERENCES

[1] "Surface Integrity of Machined Structural Components," AFML-TR-70-11, March 1970.

[2] Prevey, P. S. and Koster, W. P., in Fatigue at Elevated Temperatures, ASTM STP 520, p. 522.

[3] Williams, D. N. and Wood, R. A., "Effects of Surface Condition on the Mechanical Properties of Titanium and Its Alloys," MCIC-71-01, Aug. 1971.

[4] Leverant, G. R., Langer, B. S., Yuen, A. and Hopkins, S. W., Metallurgical Transactions, Vol. 10A, 1979, p. 251.

[5] Burck, L. H., Sullivan, C. P. and Wells, C. H., Metallurgical Transactions, Vol. 1, 1970, p. 1595.

[6] McEvily, A. J. and Johnston, T. L., International Journal of Fracture Mechanics, Vol. 3, 1967, p. 45.

[7] Garrett, G. G. and Knott, J. F., Metallurgical Transactions, Vol. 7A, 1976, p. 884.

[8] Cullity, B. D., Elements of X-Ray Diffraction, Addison-Wesley Publishing Company, Inc., Reading, Massachusetts, 1956, p. 431.

[9] Irwin, G. R., Journal of Applied Mechanics, Dec. 1962, p. 651.

[10] Broek, D., Elementary Engineering Fracture Mechanics, Noordhoff International Publishing, 1974, p. 86.

[11] Besuner, P. M., Peter, D. C. and Cipolla, R. C., "BIGIF Fracture Mechanics Code for Structures," Key Phase Report, NP-838 Research Project 700-1, EPRI, July 1978.

[12] Cruse, T. A., in The Surface Crack: Physical Problems and Computational Solutions, ASME, 1972, p. 153.

[13] Collipriest, J. E., Jr., in The Surface Crack: Physical Problems and Computational Solutions, ASME, 1972, p. 43.

[14] Hack, J. E. and Leverant, G. R., "Fatigue Microcrack Behavior under the Influence of Surface Residual Stresses," Interim Report on Contract N00014-78-C-0674, Southwest Research Institute, San Antonio, Texas, Oct. 1, 1980.

[15] Cruse, T. A., "An Improved Boundary-Integral Equation Method for Three Dimensional Elastic Stress Analysis," Interim Report on Contract DA-ARO-D-31-124-72-G3, Carnegie Mellon University, Aug. 1973.

LIST OF TABLE CAPTIONS

TABLE 1

RANGE OF ANALYZED COMPOSITIONS FOR Ti-6Al-4V MATERIAL

Element	Wt. Pct.
Al	6.3 - 6.4
V	4.3
Fe	0.10 - 0.18
O	0.17 - 0.18
N	0.013 - 0.015
H	0.005 - 0.006

TABLE 2

COMPARISON OF INDEPENDENT X-RAY STRESS MEASUREMENTS ON A SAMPLE WITH A SLIGHTLY COMPRESSIVE SURFACE RESIDUAL STRESS

	1st Run		2nd Run	
Measured Quantity	Cu K_{α_1} Peak	Cu K_{α_2} Peak	Cu K_{α_1} Peak	Cu K_{α_2} Peak
ψ=0° Peak Position (°2θ)	141.96	142.77	141.94	142.75
ψ=45° Peak Position (°2θ)	142.16	142.93	142.12	142.90
Residual Stress (MPa)	-108.33	-91.77	-98.24	-87.99

TABLE 3

CORRELATION OF MEASURED AND PREDICTED MODE I CORNER CRACK SCOD AT MAXIMUM LOAD WITH A COMPRESSIVE RESIDUAL STRESS STATE

Sample	Surface Residual Stress Value	Maximum Stress (MPa)	K_s (MPa$\sqrt{m}$)	Predicted SCOD (μ)	Measured SCOD (μ)
Ti-2	-560	500	10.1	6.0	3.8
Ti-6	-860	560	9.6	5.5	3.1
Ti-6†	≈0	560	21.5	11.2	11.3

† Stress relieved after initial experiment.

LIST OF FIGURE CAPTIONS

Figure 1 - The Microstructure of the Ti-6Al-4V Material Used in This Study. The microstructure was developed by forging at 1241°K, annealing for one hour at 1227°K, water quenching and aging for two hours at 977°K.

Figure 2 - Cantilever Beam Fatigue Specimen

Figure 3 - In-Situ Loading Stage for SEM

Figure 4 - Residual Stress Profile in Samples Ti-2 and Ti-6 (Corrected for Beam Penetration and Layer Removal)

Figure 5 - Crack Profiles in Titanium Samples. Shaded area represents region of significant residual compressive stress.

Figure 6 - Surface Crack Opening Displacement Behavior of Specimens Ti-2 and Ti-6 with Compressive Surface Stresses

Figure 7 - Micrographs of Surface Crack Opening Displacement Vs. Load in Sample Ti-6 with Compressive Surface Residual Stresses

Figure 8 - Crack Tips in Ti-6Al-4V Samples under the Influence of High Residual and Applied Loads

LIST OF FIGURE CAPTIONS (CONT.)

FIGURE 1

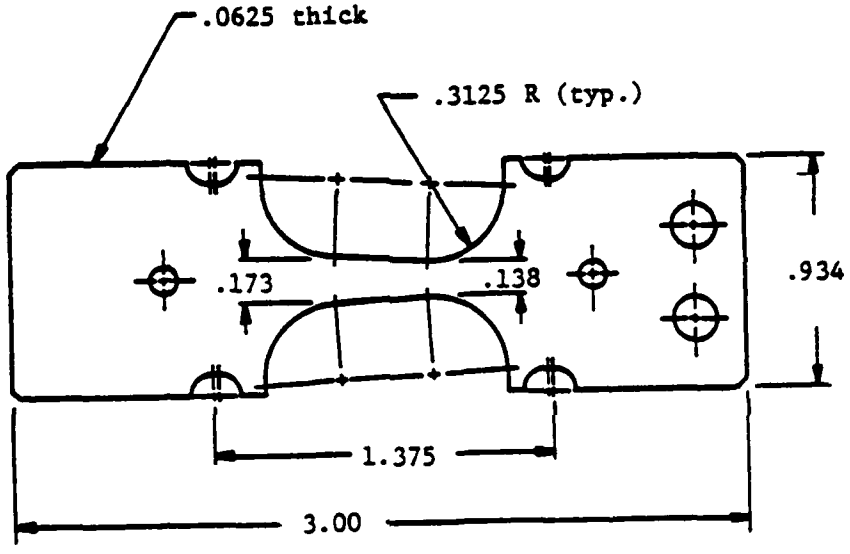

FIGURE 2

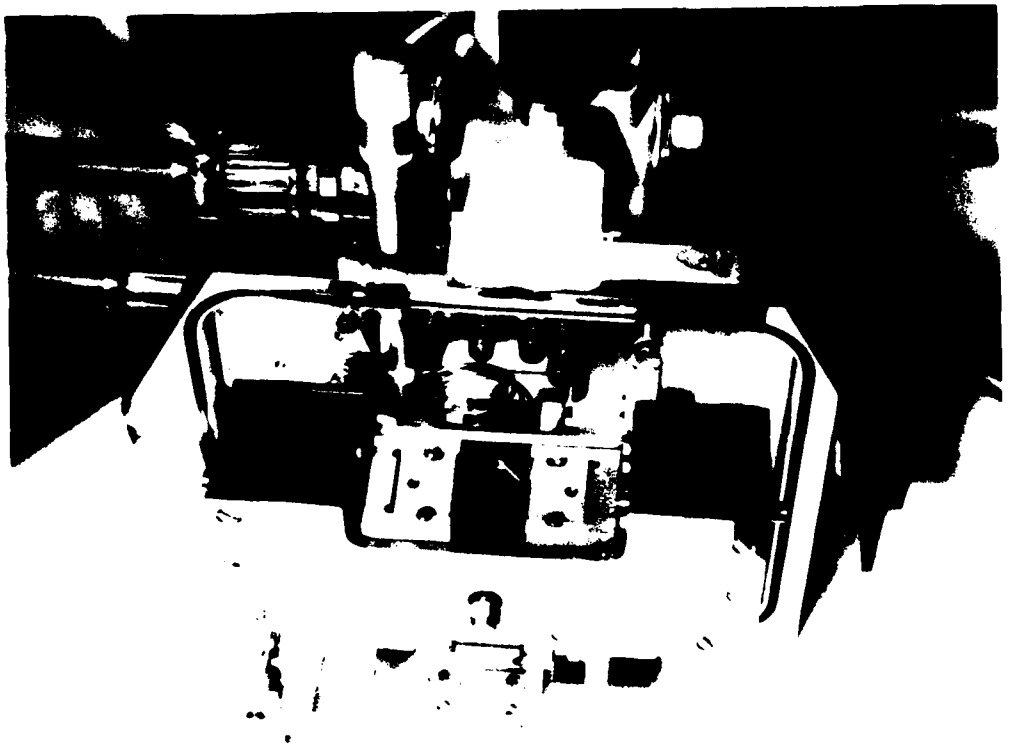

FIGURE 3

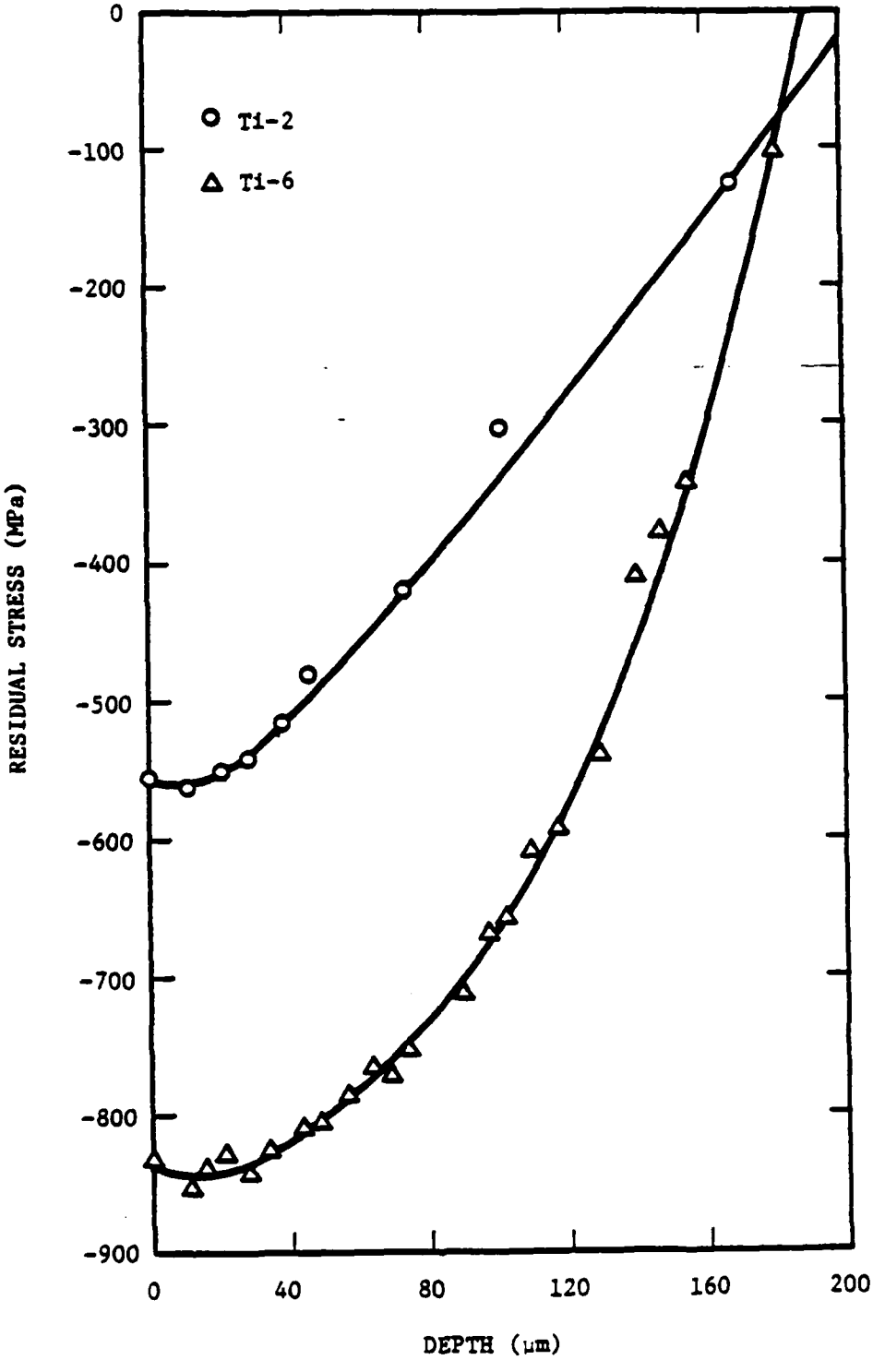
0
-100
-200
-300
-400
-500
-600
-700
-800
-900
Ti-2
Ti-6
RESIDUAL STRESS (MPa)
0
40
80
120
160
200
DEPTH (μm)

FIGURE 4

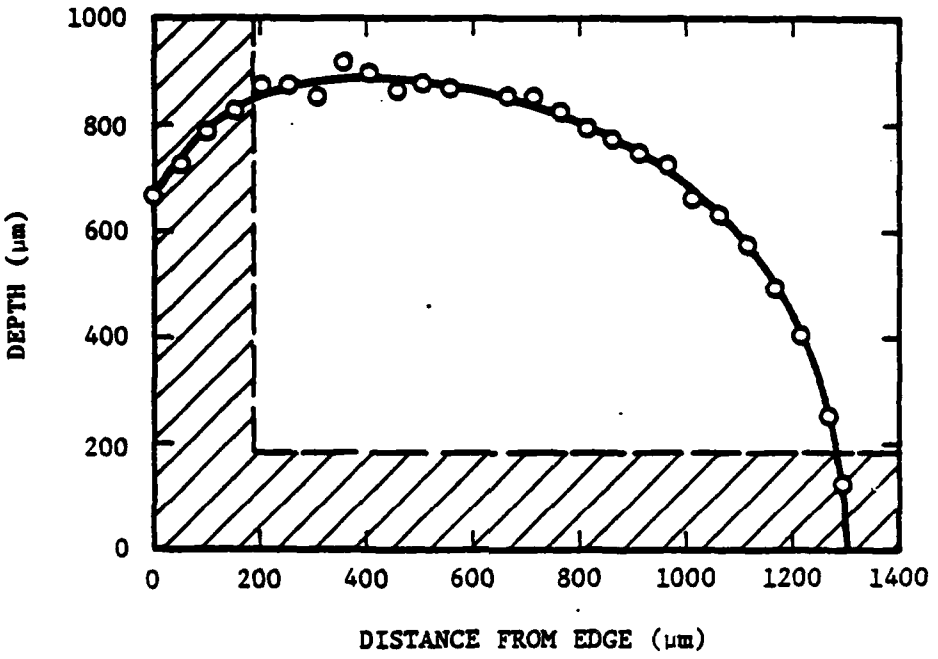

(a) Ti-2

FIGURE 5

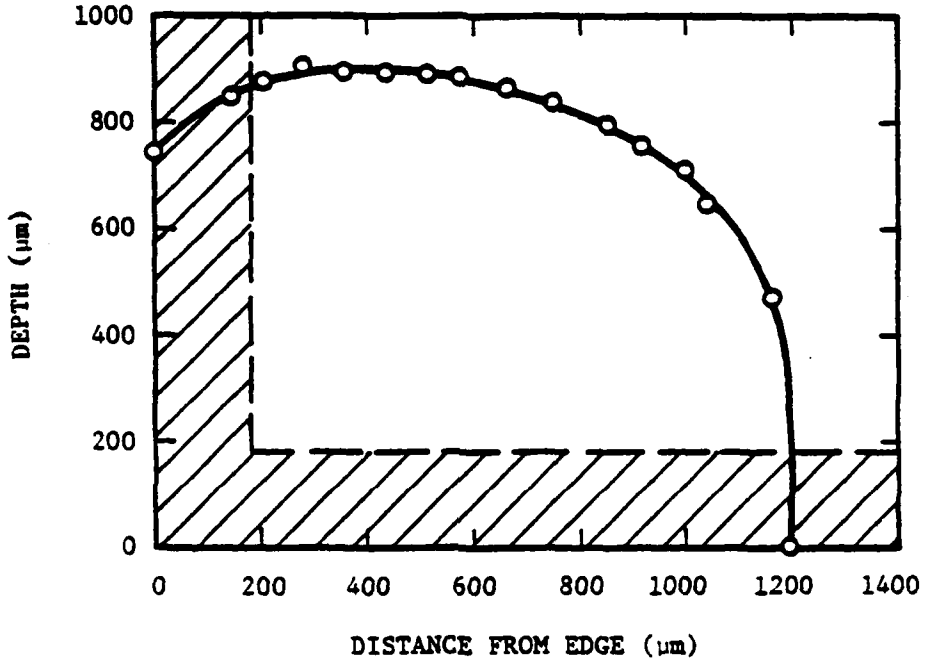

(b) Ti-6

FIGURE 5 (CONT.)

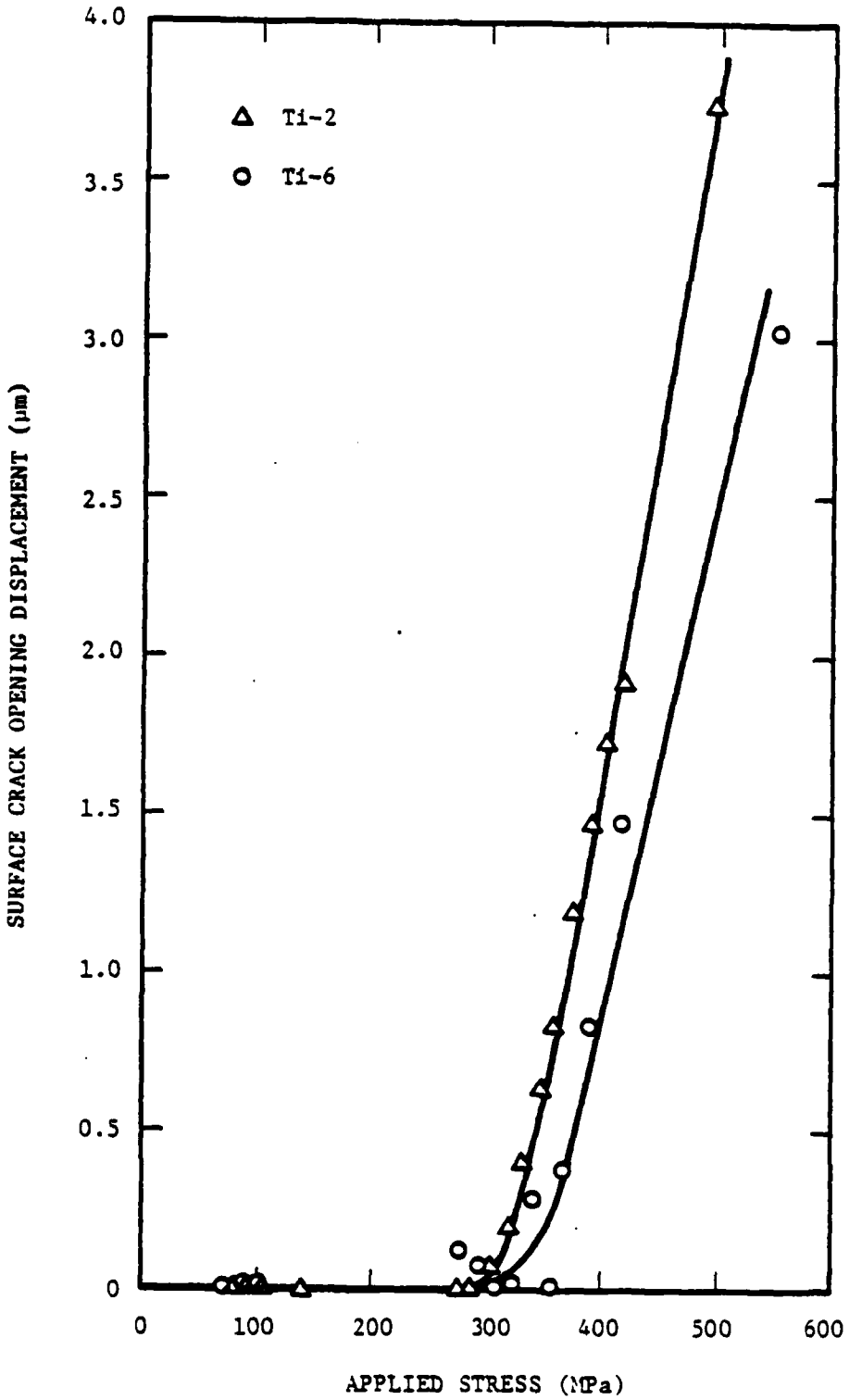
4.0
3.5
3.0
2.5
2.0
1.5
1.0
0.5
0
Ti-2
Ti-6
SURFACE CRACK OPENING DISPLACEMENT (μm)
0
100
200
300
400
500
600
APPLIED STRESS (MPa)

FIGURE 6

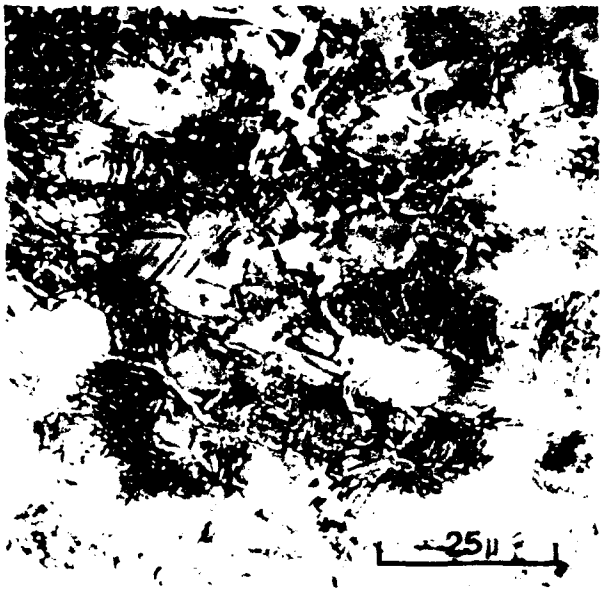

(a) 103 MPA

(b) 354 MPa

FIGURE 7

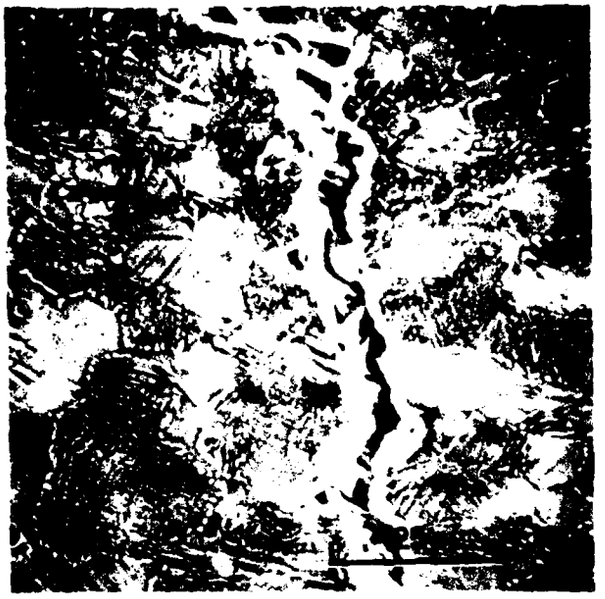

(c) 552 MPa

FIGURE 7 (CONT.)

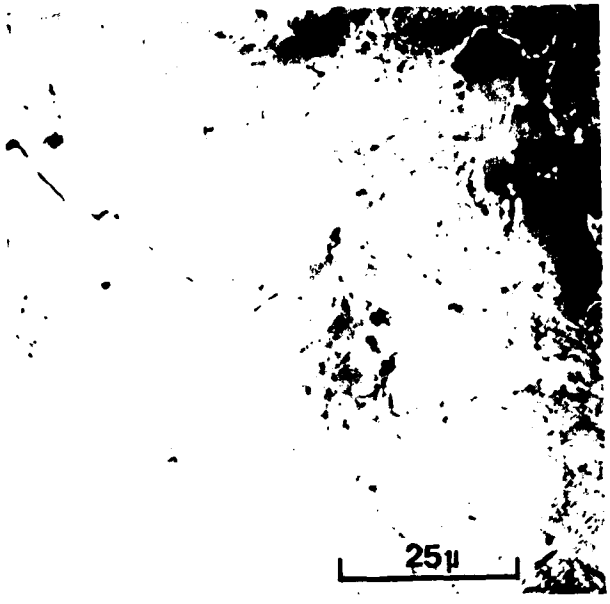

(a) Crack tip in Ti-2 at 494 MPa

(b) Crack tip in Ti-6 at 559 MPa

FIGURE 8

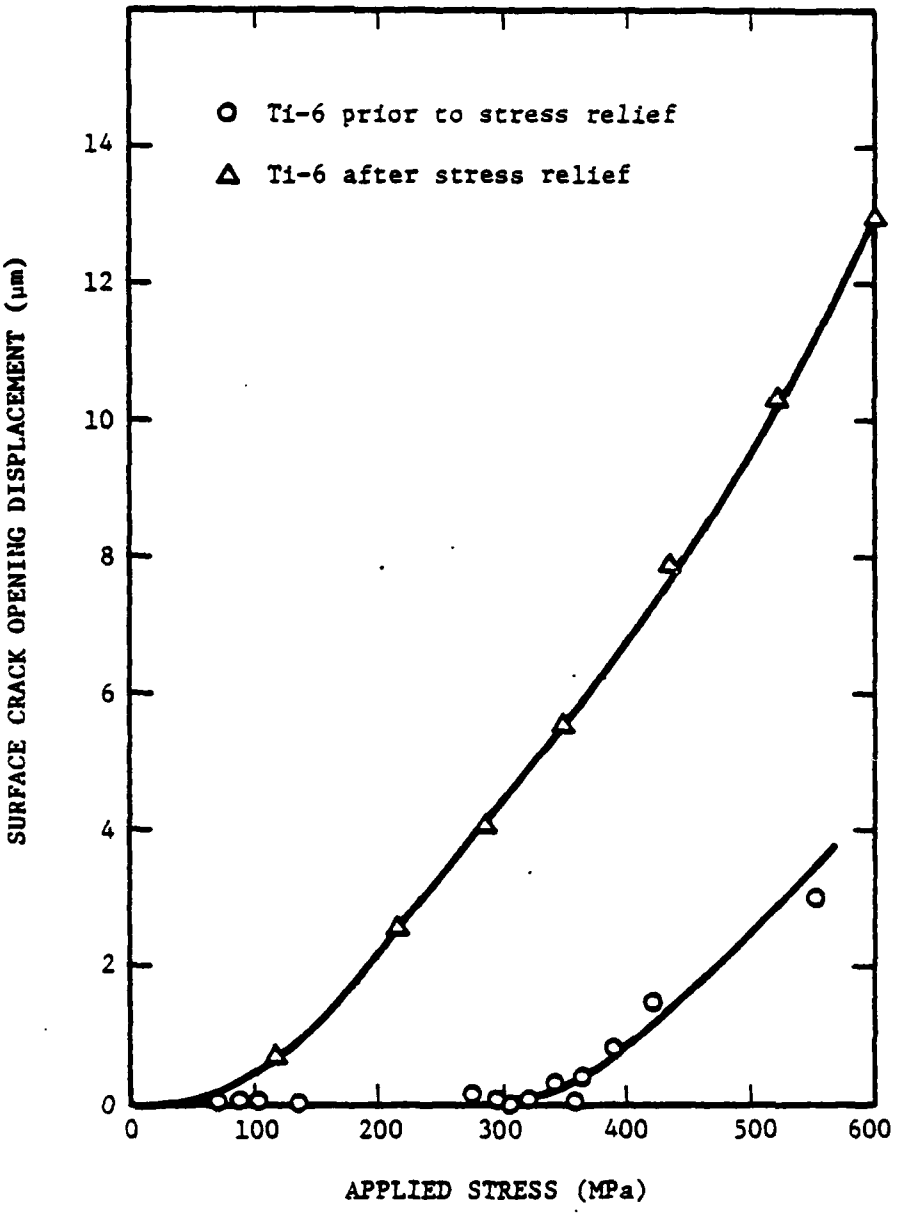
Ti-6 prior to stress relief
Ti-6 after stress relief
SURFACE CRACK OPENING DISPLACEMENT (μm)
0
2
4
6
8
10
12
14
0
100
200
300
400
500
600
APPLIED STRESS (MPa)

FIGURE 9

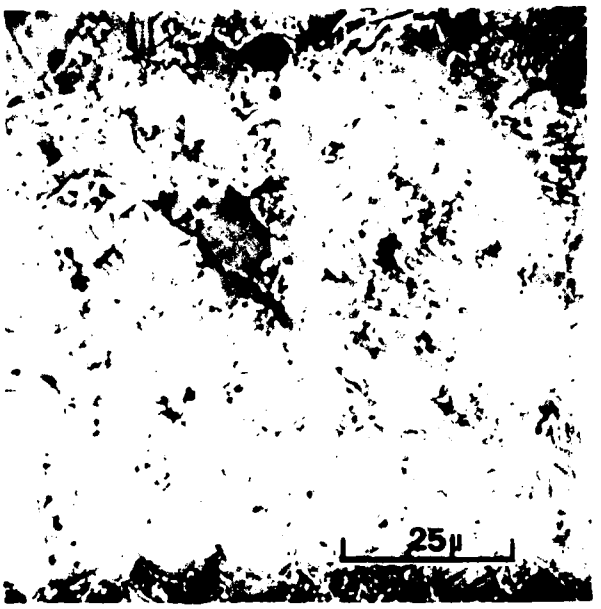

(a) Crack tip opening prior to stress relief at 408 MPa

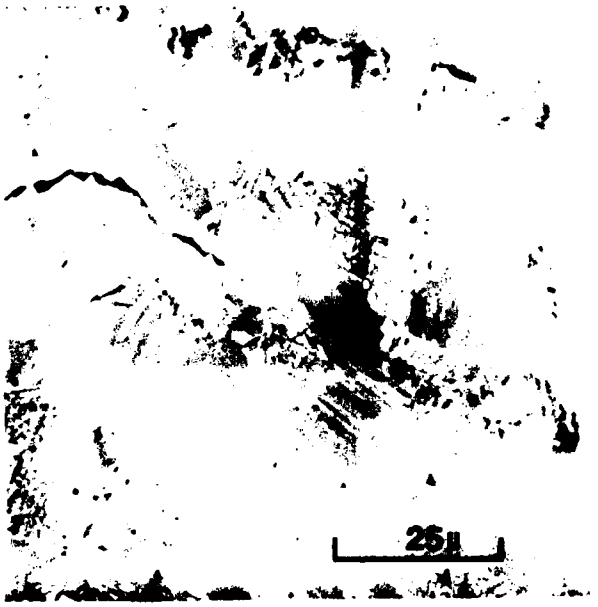

(b) Crack tip opening after stress relief at 408 MPa

FIGURE 10

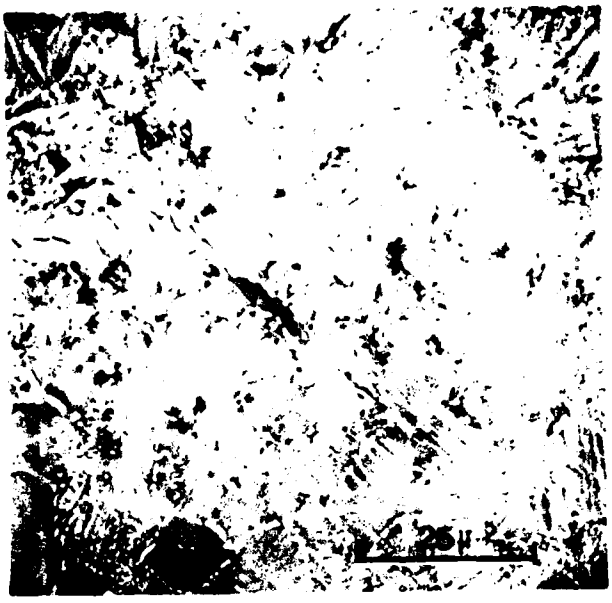

(c) Crack tip opening prior to stress relief at 559 MPa

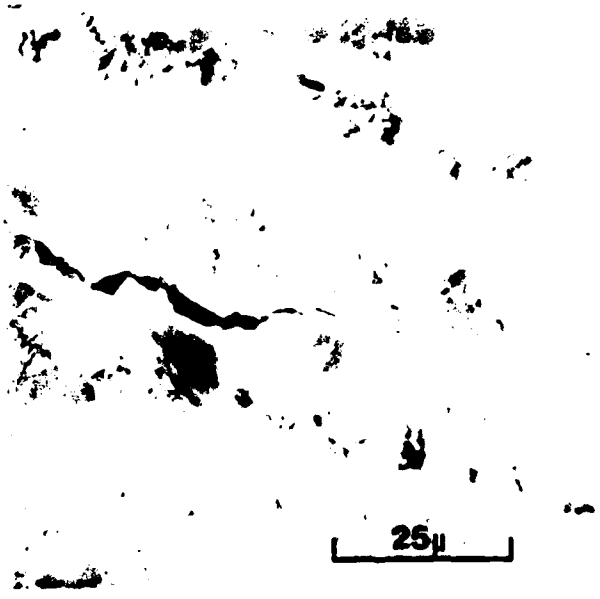

(d) Crack tip opening after stress relief at 559 MPa

FIGURE 10 (CONT.)

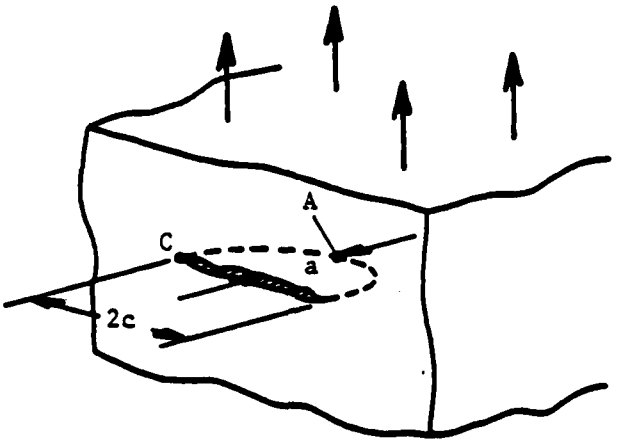

FIGURE 11

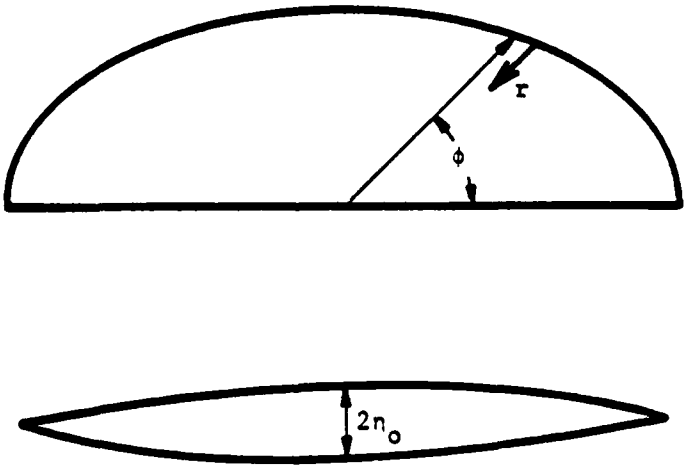

FIGURE 12

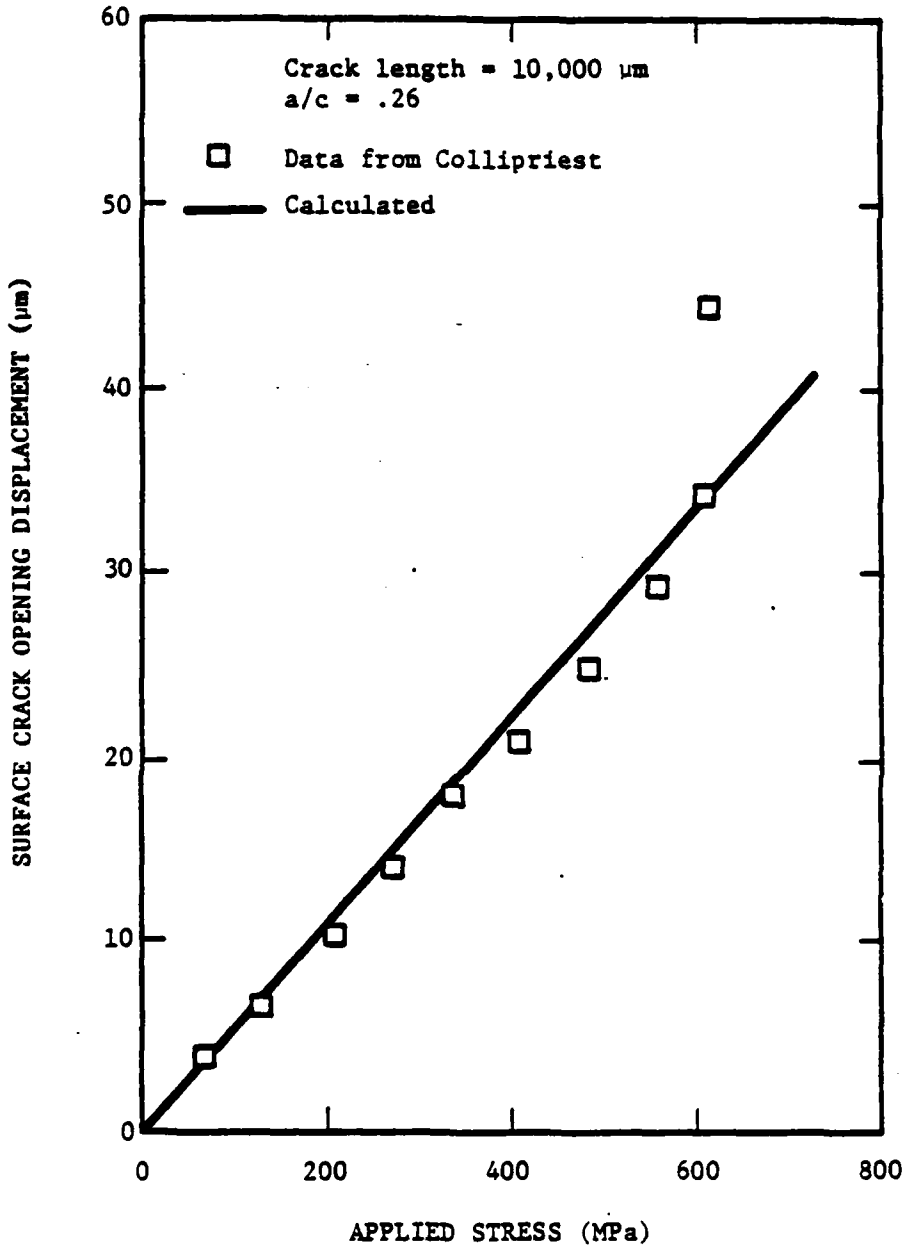
Crack length = 10,000 μm
a/c = .26
Data from Collipriest
Calculated
SURFACE CRACK OPENING DISPLACEMENT (μm)
APPLIED STRESS (MPa)
0
10
20
30
40
50
60
0
200
400
600
800

FIGURE 13

(a) 50 μ crack

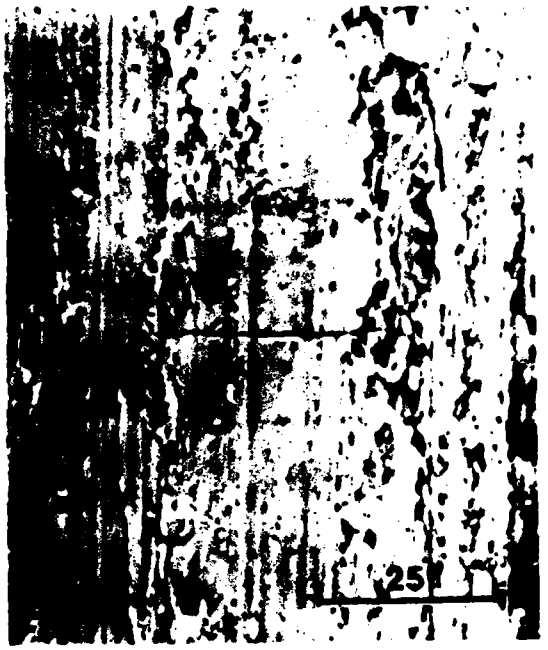

(b) 32 μ crack

FIGURE 14

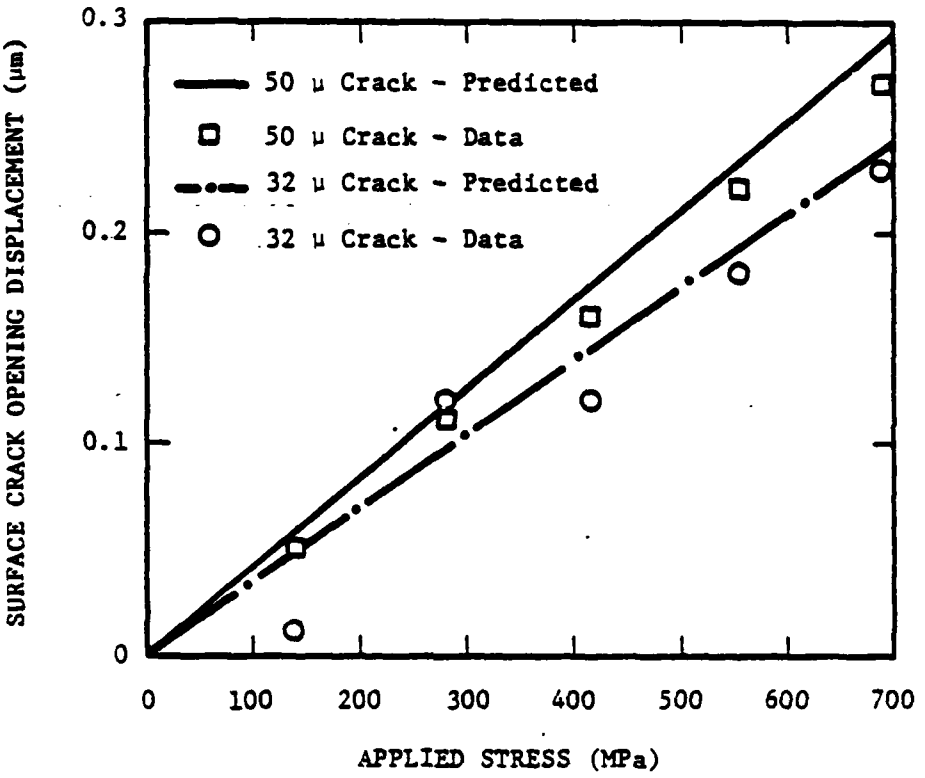
0.3
0.2
0.1
0
50 μ Crack - Predicted
50 μ Crack - Data
32 μ Crack - Predicted
32 μ Crack - Data
SURFACE CRACK OPENING DISPLACEMENT (μm)
0
100
200
300
400
500
600
700
APPLIED STRESS (MPa)

FIGURE 15